

1           **Evaluation of root water uptake in the ISBA-A-gs land surface model**  
2                           **using agricultural yield statistics over France**

3  
4           Nicolas Canal<sup>(1,2)</sup>, Jean-Christophe Calvet<sup>(1)</sup>, Bertrand Decharme<sup>(1)</sup>, Dominique Carrer<sup>(1)</sup>,  
5                           Sébastien Lafont<sup>(1,\*)</sup>, Grégoire Pigeon<sup>(3)</sup>

6  
7  
8           <sup>(1)</sup>CNRM-GAME UMR 3589 (Météo-France, CNRS), Toulouse, France

9  
10          <sup>(2)</sup>ARVALIS Institut du végétal, Service Systèmes d'Information et Méthodologies,  
11          Boigneville, France

12  
13          <sup>(3)</sup>Météo-France, Division Agrométéorologie, Toulouse, France

14  
15          <sup>(\*)</sup>now at ISPA UMR 1391 (INRA), Villenave d'Ornon, France

16

17 **Abstract**

18

19 **The simulation of root water uptake in land surface models is affected by large**  
20 **uncertainties. The difficulty in mapping soil depth and in describing the capacity of**  
21 **plants to develop a rooting system is a major obstacle to the simulation of the terrestrial**  
22 **water cycle and to the representation of the impacts of drought. In this study, long time**  
23 **series of agricultural statistics are used to evaluate and constrain root water uptake**  
24 **models. The interannual variability of cereal grain yield and permanent grassland dry**  
25 **matter yield is simulated over France by the Interactions between Soil, Biosphere and**  
26 **Atmosphere, CO<sub>2</sub>-reactive (ISBA-A-gs) generic Land Surface Model (LSM). The two**  
27 **soil profile schemes available in the model are used to simulate the above-ground**  
28 **biomass (*Bag*) of cereals and grasslands: a 2-layer force-restore (FR-2L) bulk reservoir**  
29 **model and a multi-layer diffusion (DIF) model. The DIF model is implemented with or**  
30 **without deep soil layers below the root-zone. The evaluation of the various root water**  
31 **uptake models is achieved by using the French agricultural statistics of Agreste over the**  
32 **1994–2010 period at 45 cropland and 48 grassland départements, for a range of rooting**  
33 **depths. The number of départements where the simulated annual maximum *Bag***  
34 **presents a significant correlation with the yield observations is used as a metric to**  
35 **benchmark the root water uptake models. Significant correlations (p-value < 0.01) are**  
36 **found for up to 29 % and 77 % of the départements for cereals and grasslands,**  
37 **respectively. A rather neutral impact of the most refined versions of the model is found**  
38 **with respect to the simplified soil hydrology scheme. This shows that efforts should be**  
39 **made in future studies to reduce other sources of uncertainty e.g. using a more detailed**  
40 **soil and root density profile description together with satellite vegetation products. It is**  
41 **found that modelling additional subroot zone base flow soil layers does not improve (and**

42 **may even degrade) the representation of the interannual variability of the vegetation**  
43 **above-ground biomass. These results are particularly robust for grasslands as calibrated**  
44 **simulations are able to represent the extreme 2003 and 2007 years corresponding to**  
45 **unfavourable and favourable fodder production, respectively.**

46

47

47

## 48 **1. Introduction**

49

50 Modelling the land surface processes and the surface energy, water and carbon fluxes is an  
51 important field of research in the climate community, as soil moisture and vegetation play an  
52 essential role in the climatic earth system (Seneviratne et al., 2010). A regular improvement  
53 and assessment of generic Land Surface Models (LSMs) is also required. In particular, the  
54 seasonal and interannual variability of the vegetation interacts with hydrological processes  
55 and must be represented well (Szczypta et al., 2012). Modern LSMs such as Interactions  
56 between Soil, Biosphere and Atmosphere, CO<sub>2</sub>-reactive (ISBA-A-gs) (Calvet et al., 1998;  
57 Gibelin et al., 2006) or ORganizing Carbon and Hydrology In Dynamic EcosystEms  
58 (ORCHIDEE) (Krinner et al., 2005) are able to simulate the diurnal cycle of water and carbon  
59 fluxes and, on a daily basis, plant growth and key vegetation variables such as the above-  
60 ground biomass (*Bag*) and the Leaf Area Index (LAI). In areas affected by droughts, soil  
61 moisture has a marked impact on plant growth, and the way root water uptake is represented  
62 in such LSMs may influence the simulated *Bag* and LAI values, in particular the maximum  
63 values reached every year. Therefore, long time series of observations related to the latter  
64 quantities, such as agricultural yields, have potential in the evaluation of the simulation of the  
65 Available soil Water Content (AWC) and of root water uptake in LSMs provided their  
66 interannual variability is governed by climate and not by trends or changes in agricultural  
67 practices.

68 In Europe, a marked positive trend in crops yields has been observed in the last 45 years, due  
69 to the agricultural intensification and to the evolution of farmer's practices (Smith et al.,  
70 2010a,b). However, Brisson et al. (2010) and Gate et al. (2010) have shown that yields have  
71 been stagnating in Europe since the beginning of the 1990s, and particularly since 1996 in

72 France. Therefore, it can be assumed that in the last two decades the year-to-year change in  
73 the large scale yield of a given rainfed crop type is mainly driven by the climate variability. In  
74 Europe, Smith et al. (2010a,b) showed that the agricultural statistics can be used to assess  
75 crop simulations at the country level. At a finer spatial scale over France, Calvet et al. (2012),  
76 hereafter referred to as Ca12, have used agricultural statistics (Agreste, 2014) to benchmark  
77 several configurations of the ISBA-A-gs LSM through the correlation between yield time  
78 series and *Bag* simulations for the 1994-2008 period. The Agreste data are provided for  
79 administrative units (hereafter referred to as “départements”). In ISBA-A-gs, the plant  
80 phenology is driven by photosynthesis: on a daily basis, plant growth is governed by the  
81 accumulation of the hourly net assimilation of CO<sub>2</sub> through the photosynthesis process, and  
82 plant mortality is related to a deficit in photosynthesis. The simulated annual maximum *Bag*  
83 and maximum LAI may differ from one year to another in relation to the impact of the  
84 weather and climate variability on photosynthesis. In regions where a deficit of precipitation  
85 may occur, soil moisture is a key driver of photosynthesis and plant growth of rainfed crops  
86 and grasslands. Although ISBA-A-gs is not a crop model and agricultural practices are not  
87 explicitly represented, Ca12 achieved a good representation of the interannual variability of  
88 the dry matter yield (DMY) for grasslands over many départements in France. On the other  
89 hand, representing the year to year variability of the grain yield (GY) of winter/spring cereals  
90 was more difficult. By performing a sensitivity study on different parameters of the model,  
91 they concluded that the Maximum Available soil Water Content (MaxAWC) and the  
92 mesophyll conductance in well-watered conditions ( $g_m$ ) were the two keys parameters driving  
93 the interannual variability of the simulated *Bag*. In particular, they showed that the model was  
94 markedly sensitive to MaxAWC (especially at low MaxAWC values).

95 In Ca12, an effort was made to benchmark two options of the vegetation model (drought-  
96 avoiding vs. drought-tolerant). In this study, an effort is made to benchmark several options of

97 the soil hydrology model. The main objective of this study is to assess to what extent using  
98 more refined representations of the soil hydrology and of the root water uptake can improve  
99 the representation of the interannual variability of GY (and possibly DMY). The ISBA-A-gs  
100 model and the method proposed by Ca12 are used to evaluate a new option of the ISBA-A-gs  
101 model using a multilayer soil model permitting a more detailed representation of soil moisture  
102 and soil temperature profiles, and of root water uptake. Since several options can be  
103 envisaged to implement the multilayer soil hydrology simulations, a side objective of this  
104 study is to benchmark these options and learn about the representation of root water uptake.  
105 The various versions of ISBA-A-gs are presented in Sect. 2, together with the annual yield  
106 statistics of Agreste. The symbols used in this work are listed and defined in Table 1. The  
107 results obtained with the different set of simulations are shown in Sect. 3 and the differences  
108 in the interannual variability of the various simulations of *Bag* are presented, together with the  
109 hydrological variables. The results are analyzed and discussed in Sect. 4 and the conclusions  
110 of this study are summed up in Sect. 5.

111

112

## 112 2. Data and methods

113

### 114 2.1 Agricultural statistics in France

115 Agreste is an annually updated set of agricultural data over France (Agreste, 2014). An  
116 inventory of the land use in agriculture, and of the crop, forage and livestock production is  
117 made on a yearly basis. The data are provided for départements administrative units. For  
118 crops and grasslands, annual grain yields and dry matter yields (GY and DMY, respectively)  
119 are supplied. A new version of Agreste with recalculation since 1989 has been recently  
120 published. In this study, the new Agreste dataset is used over the 1994-2010 period to  
121 examine the interannual variability of winter/spring cereal crop GY at 45 départements and of  
122 natural grassland DMY at 48 départements (Fig. 1). For cereals, we consider the six following  
123 crops: winter wheat, rye, winter barley, spring barley, oat and triticale. For grasslands, the  
124 DMY values of permanent grasslands are used. They correspond to natural grasslands or  
125 grasslands planted at least 6 years before. Figure 2 shows the interannual variability of the  
126 average GY and DMY time series derived from Agreste over the considered départements.  
127 Over the 1994-2010 period, no significant ( $p$ -value  $< 0.01$ ) trend is observed for any of the  
128 time series. A few anomalous years affected by particular climate events can be noticed. For  
129 example, Fig. 2 shows that the severe summer drought of 2003 impacted both crop and  
130 grassland yields. In 2007, the grassland production was the highest of the whole period.  
131 Conversely, it was one of the worst in terms of crop yield. The 2007 year was marked by a  
132 warm spring (favourable to permanent grasslands), followed by a slightly cold summer  
133 (detrimental to cereals). Furthermore, the rains were abundant over the grassland regions  
134 considered in this study, and have also contributed to the higher production (Agreste Bilans,  
135 2007; Agreste Conjoncture, 2007; Agreste Infos Rapides, 2007).

136

## 137 **2.2 The ISBA-A-gs land surface model**

138 The Interactions between Soil, Biosphere, and Atmosphere (ISBA) model (Noilhan and  
139 Planton, 1989; Noilhan and Mahfouf, 1996) was designed to describe the daily course of land  
140 surface state variables into global and regional climate models, weather forecast models, and  
141 hydrological models. In the original version of ISBA, a single root-zone soil layer is  
142 considered. A thin top soil layer is represented using the Deardorff (1977, 1978) force-restore  
143 approach. Soil characteristics such as soil-water and heat coefficients, the wilting point and  
144 the field capacity, depend on soil texture (sand and clay fractions). The stomatal conductance  
145 calculation is based on the Jarvis (1976) approach, and accounts for Photosynthetically Active  
146 Radiation (PAR), soil water stress, vapour pressure deficit and air temperature.

147 The representation of the soil physics of the initial version of ISBA was gradually upgraded.  
148 A multilayer soil model including soil freezing processes was developed by Boone et al.  
149 (2000) and Decharme et al. (2011). The multilayer soil model explicitly solves the one-  
150 dimensional Fourier law and the mixed-form of the Richards equation. The multilayer  
151 representation is used to discretize the total soil profile. In each layer, the temperature and the  
152 moisture are computed according to the hydrologic and texture layer characteristics. The heat  
153 and water transfers are decoupled: heat transfer is solely along the thermal gradient, while  
154 water transfer is induced by gradients in total hydraulic potential. Hereafter, the two-layer  
155 force restore model and the diffusion model are referred to as "FR-2L" and "DIF",  
156 respectively.

157 In addition to the simple Jarvis parameterization of stomatal conductance, Calvet et al. (1998)  
158 and Gibelin et al. (2006) have developed ISBA-A-gs. ISBA-A-gs ("A" stands for net  
159 assimilation of CO<sub>2</sub> and "gs" for stomatal conductance) is a CO<sub>2</sub> responsive version of ISBA  
160 able to simulate photosynthesis and its coupling to stomatal conductance. This option was

161 used in studies on the impact of climate change (Calvet et al., 2008; Queguiner et al., 2011)  
162 and on the impact of drought on the vegetation in the Mediterranean basin (Szczypta, 2012).  
163 Under well watered conditions, the A-gs formulation is based on the model proposed by  
164 Jacobs et al. (1996) (Calvet et al., 1998, 2004; Gibelin et al., 2006). In this approach, the main  
165 parameter driving photosynthesis is  $g_m$ . Under water-limited conditions, a soil moisture stress  
166 function ( $F_S$ ) is applied to key parameters of the photosynthesis model. For herbaceous  
167 vegetation, two parameters are assumed to respond to soil moisture stress (Calvet, 2000): the  
168 mesophyll conductance and the maximum leaf-to-air saturation deficit ( $D_{max}$ ). Low (high)  
169 values of the latter correspond to high (low) sensitivity of stomatal aperture to air humidity.  
170 These photosynthesis parameters are dependent on the available soil water content (AWC)  
171 scaled by its maximum value (MaxAWC). Two contrasting responses of the model  
172 parameters to soil moisture are represented: drought-avoiding and drought-tolerant (see  
173 Supplement 1). When the AWC/MaxAWC ratio is higher than the critical soil water stress  
174  $F_{SC}$  ( $F_{SC} = 0.3$  in our simulations), a drop in AWC triggers an increase (decrease) in  $g_m$  and a  
175 decrease (increase) in  $D_{max}$  for the drought-avoiding (drought-tolerant) parameterization. The  
176 drought-avoiding parameterization is used for cereal crops and the drought-tolerant  
177 parameterization is used for grasslands. This assumption was validated by Ca12. The drought  
178 response model is illustrated by Fig. S1 in Supplement 1. These parameters are then used to  
179 calculate the hourly leaf-level net assimilation of  $CO_2$  and the stomatal conductance, in  
180 relation to sub-daily meteorological inputs such as the incoming solar radiation. A radiative  
181 transfer scheme is then used to upscale net assimilation of  $CO_2$  and transpiration at the  
182 vegetation level. The plant transpiration flux is used to calculate the soil water budget through  
183 the root water uptake. The net assimilation of  $CO_2$  serves as an input to the plant growth  
184 model, and LAI and  $B_{ag}$  are updated on a daily basis. Figure 3 illustrates these mechanisms.  
185 For moderate soil water stress, the drought-avoiding response results in the increase of the

186 Water Use Efficiency (WUE). In the drought-tolerant response, WUE does not change or  
187 decreases. **It must be noted that another** representation of the response to drought is used for  
188 forests (Calvet et al., 2004).

189 ISBA-A-gs contains a photosynthesis-driven plant growth model able to simulate LAI and the  
190 vegetation biomass on a daily basis. For herbaceous vegetation, the model simulates the  
191 above-ground biomass. The *Bag* variable has two components (active biomass and structural  
192 biomass) related by a nitrogen dilution parameterization (Calvet and Soussana, 2001). The  
193 leaf nitrogen concentration  $N_L$  is a parameter of the model affecting the Specific Leaf Area  
194 (SLA), the ratio of LAI to leaf biomass (in  $\text{m}^2 \text{kg}^{-1}$ ). The SLA depends on  $N_L$  and on plasticity  
195 parameters (Gibelin et al., 2006). This version of ISBA-A-gs, called "NIT", is used in this  
196 study.

197 An assessment of the quality of ISBA-A-gs outputs variables has been performed in previous  
198 local studies with in-situ data over France (Rivalland et al., 2005; de Rosnay et al., 2006;  
199 Sabater et al., 2007; Brut et al., 2009; Lafont et al., 2012). Gibelin et al. (2006) have shown  
200 that the LAI simulated by ISBA-A-gs at a global scale is consistent with satellite-derived LAI  
201 products.

202 Furthermore, a radiative transfer model within the vegetation canopy describes the attenuation  
203 of the PAR through a self-shading approach and photosynthesis is calculated at three levels of  
204 the canopy using a three-point Gauss quadrature method (Jacobs, 1994). A New Radiative  
205 Transfer (hereafter referred to as "NRT") scheme was recently implemented in ISBA-A-gs by  
206 Carrer et al. (2013). The NRT is more detailed than the original model and a vertical profile  
207 of ten layers within the canopy is represented. Because of the heterogeneity of the different  
208 vegetation canopies, distinct bottom and top canopy layer parameterizations are considered.  
209 Also, NRT has distinct representations of sunlit and shaded leaves, with two PAR calculations

210 at each layer. Carrer et al. (2013) showed that NRT represents better the Gross Primary  
 211 Production (GPP) at both local and global scales.

### 212 **2.3 Root density and the soil water stress**

213 In the DIF simulations, the root density profile ( $Y$ ) is expressed by the following equation  
 214 derived from Jackson et al. (1996):

$$216 \quad Y(d_L) = \frac{1 - R_e^{100 \times d_L}}{1 - R_e^{100 \times d_R}} \quad (1)$$

217 where  $Y(d_L)$  is the cumulative root fraction (a proportion between 0 and 1) from the soil  
 218 surface to the bottom of a soil layer within the root-zone, at a depth  $d_L$  (m),  $d_R$  is the root-zone  
 219 depth (m) and  $R_e$  the root extinction coefficient equal to 0.961 and 0.943 for crops and for  
 220 temperate grasslands, respectively (Jackson et al., 1996). For a given value of  $d_R$ , the lower  
 221 value of  $R_e$  for temperate grasslands corresponds to a cumulative root fraction higher than for  
 222 crops close to the top soil layer, 15 % higher at  $d_L = 0.36$  m, more than 40 % higher at  $d_L <$   
 223 0.05 m. The cumulative root density is equal to 1 at the bottom of the root-zone soil layer  
 224 ( $d_R$ ).

225 The Soil Wetness Index of a top soil layer of thickness  $d_L$  and of a soil layer at depth  $d_{Li}$   
 226 ( $SWI_{TOP}$  and  $SWI$ , respectively) are defined as:

$$228 \quad SWI_{TOP}(d_L) = (\theta_{TOP}(d_L) - \theta_{TOP,WILT}) / (\theta_{FC,TOP} - \theta_{WILT,TOP}) \quad (2)$$

$$229 \quad SWI(d_{Li}) = (\theta(d_{Li}) - \theta_{WILT}(d_{Li})) / (\theta_{FC}(d_{Li}) - \theta_{WILT}(d_{Li})) \quad (3)$$

230  
 231 where  $\theta_{TOP}(d_L)$  and  $\theta(d_L)$  are the volumetric water content (in  $m^3 m^{-3}$ ) of a top soil layer of  
 232 thickness  $d_L$  and at depth  $d_L$ , respectively, and the subscript "FC" and "WILT" indicate soil  
 233 moisture at field capacity and at wilting point, respectively. Equation (2) is used to assess the

234 soil moisture stress in a single soil layer or in several soil layers forming a bulk layer from the  
 235 surface to a depth  $d_L$ . Equation (3) is used to assess the soil moisture stress of an individual  
 236 soil layer at depth  $d_{Li}$ . Equation (2) and Eq. (3) are used to calculate the stress function in FR-  
 237 2L and DIF simulations, respectively. In this study, the same soil type is used for all the  
 238 simulations, and an homogeneous soil profile is assumed with sand and clay fractions of 32.0  
 239 % and 22.8 %, respectively, and  $\theta_{FC} = \theta_{TOP,FC} = 0.30 \text{ m}^3 \text{ m}^{-3}$  and  $\theta_{WILT} = \theta_{TOP,WILT} = 0.17 \text{ m}^3$   
 240  $\text{m}^{-3}$ . Since the agricultural statistics we use concern rather large administrative units, it would  
 241 have been illusory to try and use local soil texture properties.  
 242 The value of MaxAWC is expressed in units of  $\text{kg m}^{-2}$  and depends on soil and plant  
 243 characteristics: soil moisture at field capacity, soil moisture at wilting point ( $\theta_{FC}$  and  $\theta_{WILT}$ ,  
 244 respectively, in  $\text{m}^3 \text{ m}^{-3}$ ) and rooting depth ( $d_R$ , in m):

$$246 \text{MaxAWC} = \rho (\theta_{FC} - \theta_{WILT}) d_R \quad (4)$$

247  
 248 where  $\rho = 1000 \text{ kg m}^{-3}$  is the water density. The  $\theta_{FC}$  and  $\theta_{WILT}$  values are common to all the  
 249 simulations and the different MaxAWC values are obtained by varying the root-zone depth  
 250 ( $d_R$ ).

251 In the ISBA-A-gs simulations, the dimensionless stress function  $F_S$  is used to calculate  
 252 photosynthesis and the plant transpiration flux ( $F_T$ , in  $\text{kg m}^{-2} \text{ s}^{-1}$ ). The  $F_S$  function varies  
 253 between 0 (at wilting point or below) and 1 (at field capacity or above). Between these two  
 254 limits,  $F_S = \text{SWI}_{TOP}(d_R)$  in FR-2L and plant transpiration is driven by the total soil water  
 255 content in the root-zone. In the case of DIF simulations,  $F_S$  is the sum of the stress functions  
 256 of each soil layer in the root-zone  $F_S(i)$ , i.e.  $\text{SWI}(d_{Li})$ , balanced by the root fraction  $R_d$  at  
 257 depth  $d_{Li}$ :

258

259 
$$F_s(i) = SWI(d_{L_i}) \times \frac{R_d(d_{L_i})}{\sum_{j=1}^N R_d(d_{L_j})}, \text{ and } F_s = \sum_{i=1}^N F_s(i) \quad (5)$$

260

261 where  $N$  is the number of soil layers in the root-zone. Once the  $F_s$  stress index has been  
 262 determined, the photosynthesis parameters can be updated, and the leaf-level and vegetation-  
 263 level fluxes can be calculated (Fig. 3).

264 The root water uptake in layer  $i$ ,  $S_T(i)$  (in  $\text{kg m}^{-2} \text{s}^{-1}$ ), is calculated as:

265

266 
$$S_T(i) = F_T \times F_s(i) / F_s \quad (6)$$

267

## 268 2.4 Design of the simulations

269 In this study, the ISBA-A-gs LSM is used within version 7.2 of the SURFEX (“SURFace  
 270 EXternalisée”) Earth surface modelling platform of Météo-France (Masson et al., 2013). For  
 271 the first time, the NIT biomass option of the model and the NRT light absorption scheme are  
 272 used together with the DIF multilayer soil configuration. Two representations of the soil  
 273 hydrology (FR-2L and DIF options) are considered, for both C3 crops and grasslands. The  
 274 model simulations are offline (not coupled with the atmosphere) and driven by a  
 275 meteorological reanalysis. We consider that the vegetation cover fraction is equal to 1 across  
 276 seasons. We use the ISBA-A-gs default avoiding (tolerant) response to the drought for C3  
 277 crops (grasslands). Standard values of the model parameters used in this study are  
 278 summarized in Table 2.

279 Six experiments are performed:

- 280 • FR-2L, is based on the force-restore representation of the soil hydrology and is similar  
 281 to the model configuration used by Ca12. The root-zone corresponds to the whole soil  
 282 layer.

- 283 • DIF1 uses the new DIF capability of SURFEX v7.2 (Fig. 4). As in FR-2L, the root-  
284 zone corresponds to the whole soil layer. The root-profile reaches the bottom of the  
285 soil layer and the total soil depth corresponds to  $d_R$ .
- 286 • DIF2 includes additional subroot zone base flow soil layers with respect to DIF1 and  
287 the deep soil layers contribute to plant transpiration through **capillary** rises. It is  
288 assumed that MaxAWC is governed by the limited capacity of the plants to develop a  
289 root system in a deep soil and the number of subroot zone layers decreases when the  
290 rooting depth increases. A constant total soil depth of 1.96 m is prescribed and  $d_R$  is  
291 varied between 0.36 m and 1.76 m (Fig. 5).
- 292 • DIF3 is similar to DIF1, as soil depth is the main limitation of root water extraction.  
293 However, two additional base flow soil layers contribute to transpiration through  
294 **capillary** rises. The total soil depth and  $d_R$  are varied simultaneously, and two adjacent  
295 0.1 m thick deep soil layers are represented (Fig. 6).
- 296 • DIF1-NRT permits assessing the impact of a refined representation of the CO<sub>2</sub> uptake  
297 by the vegetation on the *Bag* interannual variability, as the NRT light absorption  
298 option is used together with DIF1.
- 299 • DIF1-Uniform permits assessing the sensitivity of the ISBA-A-gs simulations to the  
300 shape of the root density profile. It corresponds to DIF1 simulations using a uniform  
301 root density profile instead of Eq. (1). These simulations are made over the 61-Orne  
302 département (see Sect. 4.1).

## 303 **2.5 Atmospheric forcing**

304 The atmospheric forcing data required for our simulations are provided by the SAFRAN  
305 (“Système d’Analyse Fournissant des Renseignements Atmosphériques à la Neige”) mesoscale  
306 atmospheric analysis system (Durand et al., 1993, 1999). Precipitation, air  
307 temperature, air humidity, wind speed, incoming solar radiation and incoming infrared

308 radiation are provided over France at  $8 \text{ km} \times 8 \text{ km}$  spatial resolution on an hourly basis. The  
309 SAFRAN product was evaluated by Quintana-Seguí et al. (2008) using independent in situ  
310 observations. One-dimensional model simulations are performed at the  $8 \text{ km} \times 8 \text{ km}$  spatial  
311 resolution of SAFRAN, at grid cells corresponding to cereal and natural grassland  
312 départements (Fig. 1). These grid cells correspond to plots located within a département and  
313 with at least 45% of their surface covered by either grasslands or crops, according to the  
314 average plant functional type coverage given by the  $1 \text{ km} \times 1 \text{ km}$  ECOCLIMAP-II global data  
315 base (Faroux et al., 2013).

## 316 2.6 Optimisation of two key parameters

317 In this study, the method proposed by Ca12 is used: the values of two key parameters of the  
318 ISBA-A-gs simulations, MaxAWC and  $g_m$ , are explored and the parameter pair providing the  
319 best correlation coefficient ( $r$ ) of the maximum annual value of  $Bag$  ( $Bag_x$ ) and GY (DMY) is  
320 selected, for C3 crops (grasslands). For the FR-2L experiment, the optimisation of both  
321 MaxAWC and  $g_m$  is performed for all the départements of Fig. 1. For the DIF1, DIF2, and  
322 DIF3 experiments, only MaxAWC is optimised and the  $g_m$  values derived from the FR-2L  
323 optimisation are used. In the case of crops, simulated  $Bag$  values after 31 July are not  
324 considered, in order to be consistent with the theoretical averaged harvest dates in France.  
325 Attempts were made to use other dates in July (not shown), without affecting the results of the  
326 analysis. On the other hand, new optimal  $g_m$  values are obtained together with MaxAWC for  
327 the DIF1-NRT experiment, as the representation of photosynthesis at the canopy level differs  
328 from the other experiments. Moreover, major differences with Ca12 are that (1) a longer  
329 period is considered (1994-2010 instead of 1994-2008 in Ca12); (2) a more detailed screening  
330 of MaxAWC values is performed (12 values are considered, against 8 values in Ca12).

331 For all the experiments, MaxAWC ranges between 50 and 225 mm, with a lower increment  
 332 between the small values (50, 62.5, 75, 87.5, 100, 112.5, 125, 137.5, 150, 175, 200 and 225  
 333 mm, 12 in total).

334 For the  $g_m$  parameter, the same range of values as in Ca12 is used (from 0.50 mm s<sup>-1</sup> to 1.75  
 335 mm s<sup>-1</sup>, 6 in total). For the three simulations DIF1, DIF2 and DIF3, the same values of  
 336 optimal  $g_m$  obtained for each **département** and vegetation type with the FR-2L version are  
 337 used.

## 338 **2.7 Metrics used to quantify the interannual variability**

339 In Section 4, the following metrics are used: the Annual Coefficient of Variation (ACV),  
 340 computed as the ratio of the standard deviation ( $\sigma$ ) of the simulated  $Bag_x$  to the long term  
 341 mean  $Bag_x$ ,

$$342 \quad ACV = \frac{\sigma(Bag_x)}{Bag_x} \quad (7)$$

343

344 the scaled anomaly ( $A_S$ ) of  $Bag_x$  of a given year ( $yr$ ):

345

$$346 \quad A_{S,Bag_x}(yr) = \frac{Bag_x(yr) - \overline{Bag_x}}{\sigma(Bag_x)} \quad (8)$$

347

348 This metric is also called z-score and can be applied to the Agreste cereal GY:

$$349 \quad A_{S,GY}(yr) = \frac{GY(yr) - \overline{GY}}{\sigma(GY)} \quad (9)$$

350

351 and to the Agreste grassland DMY:

$$352 \quad A_{S,DMY}(yr) = \frac{DMY(yr) - \overline{DMY}}{\sigma(DMY)} \quad (10)$$

353

354

### 355 **3. Results**

356

#### 357 **3.1 Interannual variability of $Bag_x$ values**

##### 358 **3.1.1 DIF1 vs. FR-2L**

359 Figures 7 and 8 show an example of the interannual variability of the simulated  $Bag$  and  
360 AWC (in  $\text{kg m}^{-2}$ ) as simulated by FR-2L and DIF1 for C3 crops and grasslands of the 61-  
361 Orne département. The optimal parameter values for C3 crops and grasslands are  $1.75 \text{ mm s}^{-1}$   
362 and  $0.5 \text{ mm s}^{-1}$  for  $g_m$ , and 200 mm and 50 mm for MaxAWC, respectively.

363 For C3 crops (Fig. 7),  $Bag_x$  values for FR-2L tend to reach slightly higher values than for  
364 DIF1. The largest difference is observed in 1996. Furthermore, some differences occur in the  
365 senescence period, especially in 2001 and 2009. Conversely, the simulated AWC values are  
366 higher for DIF1, especially in winter. For both simulations, the wintertime AWC is often  
367 higher than MaxAWC (set to 200 mm), in relation to water accumulation above field  
368 capacity, in wet conditions. This phenomenon is more pronounced for DIF1 than for FR-2L.  
369 A crop regrowth is simulated by both FR-2L and DIF1 during years with a marked summer  
370 drought, in 1995, 1996, 1998, 2006 and 2010. During wet years (i.e. in 1994, 2000 and 2007),  
371 the two experiments provide similar AWC values at summertime.

372 For grasslands (Fig. 8), the two  $Bag$  simulations are also very close. However, contrary to C3  
373 crops, the  $Bag$  values of the FR-2L simulation tend to be slightly lower than the DIF1 ones  
374 (e.g. in 1997, 2002, 2007, and 2009). The other difference with C3 crops is the systematic  
375 occurrence of regrowths.

##### 376 **3.1.2 ISBA-A-gs simulations vs. Agreste observations**

377 The départements where FR-2L  $Bag_X$  simulations present significant ( $p$ -value  $< 0.01$ )  
378 correlations with the Agreste GY and DMY time series are presented in Fig. 9, and the  
379 retrieved  $g_m$  and MaxAWC median values are presented in Table 3 for all the experiments,  
380 together with the number of départements presenting significant correlations with Agreste, for  
381 C3 crops and grasslands. With FR-2L, 12 (5) départements present significant positive  
382 correlations at the 1% (0.1%) level for C3 crops. For grasslands, 34 (22) départements present  
383 significant positive correlations at the 1% (0.1%) level. Although the considered period is  
384 longer than in Ca12 (17 yr instead of 15 yr), these results are similar to those presented in  
385 Ca12, even if slight differences can be noticed, such as the number of départements with a  
386 significant correlation. In DIF simulations for C3 crops, DIF1 and DIF3 perform nearly as  
387 well as FR-2L, and they outperform DIF2: 10 (3) départements present significant positive  
388 correlations at the 1% (0.1%) level for both DIF1 and DIF3, against 6 (2) for DIF2. For the  
389 grasslands, a larger proportion of départements (among 48) presents significant correlations,  
390 from 27 (10) départements for DIF2 to 36 (20) for DIF1. The addition of deep soil layers  
391 below the root zone tends to degrade the results, especially in DIF2. Finally, the DIF1-NRT  
392 simulations perform as well as FR-2L or better with 13 (4) and 37 (19) départements  
393 presenting significant positive correlations at the 1% (0.1%) level for C3 crops and  
394 grasslands, respectively.

395 Selecting the départements where the optimisation is successful, i.e. where the correlation  
396 between  $Bag_X$  and GY or DMY is significant ( $p$ -value  $< 0.01$ ), the time series of the mean  
397  $Bag_X$  and mean GY and of the mean  $Bag_X$  and mean DMY are compared in Fig. 10 for both  
398 FR-2L and DIF1-NRT experiments. The interannual variability of the grassland DMY is  
399 better represented by  $Bag_X$  than for the cereal GY, with  $R^2 = 0.83$  and  $R^2 = 0.45$ , respectively.  
400 The FR-2L experiment presents slightly better  $R^2$  values than DIF1-NRT. For C3 crops, it  
401 appears that the two experiments are not able to represent the lower GY in 2007, nor the

402 higher GY in 2004. For grasslands, the two experiments are not able to represent the lower  
403 DMY in 1996.

## 404 3.2 Impact of subroot zone soil layers

### 405 3.2.1 Optimal MaxAWC values

406 Table 3 shows that for C3 crops, the median MaxAWC value is higher for FR-2L than for  
407 DIF1 (125.0 mm and 112.5 mm, respectively). For DIF2 and DIF3, the median MaxAWC is  
408 even lower (81.3 mm and 93.8 mm, respectively). For grasslands, the median MaxAWC is  
409 less variable from one experiment to another (from 68.8 mm to 81.3 mm). In Table 3, the  
410 median MaxAWC values are calculated irrespective of which Agreste cereal GY values are  
411 used to derive MaxAWC. Among the 10 départements with DIF1 simulations presenting  
412 significant correlations at the 1 % level with Agreste, 8 départements share the same cereal  
413 Agreste yields with FR-2L.

414 These 8 départements are listed in Table 4 together with squared correlation coefficient ( $R^2$ )  
415 values and MaxAWC for FR-2L and DIF1. The FR-2L  $R^2$  is higher than the DIF1  $R^2$ , except  
416 for 08-Ardenne and 63-Puy-de-Dôme. Again, the median MaxAWC is higher for FR-2L than  
417 for DIF1 (118.8 mm and 112.5 mm, respectively). The FR-2L MaxAWC value is lower than  
418 the DIF1 MaxAWC value only once, for the 61-Orne département. This indicates that the  
419 DIF1 root density profile tends to increase the impact of drought on plant growth for this  
420 département. Also, the largest difference in  $R^2$  between FR-2L and DIF1 is observed for this  
421 département.

### 422 3.2.2 Plant growth

423 Table 3 shows that in DIF2 simulations the number of départements with a significant  
424 correlation at the 1% level is lower than in other experiments. The use of DIF2 has a  
425 detrimental impact on the representation of the interannual variability by the plant growth  
426 model. Figure 11 shows the impact of the root water uptake model on the simulated C3 crop

427 *Bag* and root-zone soil moisture for the 08-Ardennes département during the growing season,  
428 from April to July 1996. In the FR-2L, DIF1, DIF2, and DIF3 simulations shown in Fig. 11,  
429 the same  $g_m = 0.5 \text{ mm s}^{-1}$  and  $\text{MaxAWC} = 75 \text{ mm}$  values are used. The growth period is  
430 longer in the DIF2 simulation than in the other ones, with senescence starting only during the  
431 second half of July. At the same time, the DIF2 root-zone soil moisture presents the highest  
432 values. It appears that in the DIF2 simulation, the additional water supplied by capillary rises  
433 from the subroot zone soil layers has a marked impact on the phenology, with the date of  
434 maximum *Bag* shifted to the end of July and a much higher  $Bag_x$  value than in the other  
435 experiments ( $1.02 \text{ kg m}^{-2}$  for DIF2, against  $0.62 \text{ kg m}^{-2}$ ,  $0.58 \text{ kg m}^{-2}$ ,  $0.72 \text{ kg m}^{-2}$  for FR-2L,  
436 DIF1, and DIF3, respectively). The same phenomenon happens in the DIF3 simulation to a  
437 lower extent. In particular, the DIF3  $Bag_x$  is not very different from the FR-2L one. The DIF1  
438 simulation is closer to FR-2L. When the root-zone soil moisture reaches the wilting point  
439 (equal to  $0.17 \text{ m}^3 \text{ m}^{-3}$  as indicated in Fig. 11 by the dashed line), the senescence starts. A  
440 marked water stress occurs and impacts photosynthesis and biomass production. Since water  
441 is supplied by the subroot zone soil layers of DIF2 and DIF3, the wilting point is reached later  
442 than for FR-2L and DIF1 and the senescence starts later.

443 In FR-2L, the growth of *Bag* is faster than in the other simulations. This leads to a slightly  
444 higher value of  $Bag_x$  than for DIF1. This is related to the lower FR-2L root-zone soil moisture  
445 in May. In the drought-avoiding C3 crop parameterization of ISBA-A-gs, a moderate soil  
446 moisture stress triggers an increase in water use efficiency (Calvet, 2000) and enhances plant  
447 growth.

448

## 449 **4. Discussion**

450

### 451 **4.1 Is the Jackson root profile model (Eq. (1)) applicable at the regional scale ?**

452 In the DIF simulations, the stress function depends on the distribution of root density through  
453 Eqs. (5)-(6). This allows the lower layers to sustain the transpiration rate to some extent when  
454 the upper soil layers dry out. However, one may emphasize that the approach used in this  
455 study to simulate the root water uptake is relatively simple and may not be relevant to  
456 represent what really happens at a regional scale. Higher level models are able to simulate the  
457 root network architecture and the three dimensional soil water flow (Schneider et al. 2010,  
458 Jarvis 2011). Also, the hydraulic redistribution of water from wetter to drier soil layers by the  
459 root system (hydraulic lift) is not simulated in this study. Siquiera et al. (2008) have  
460 investigated the impact of hydraulic lift using a detailed numerical model and showed that this  
461 effect could be significant.

462 Another difficulty in the implementation of DIF simulations is that the proposed  $R_e$  values in  
463 Eq. (1) are the result of a meta-analysis. A single  $R_e$  value is proposed for a given vegetation  
464 type while a large variability of  $R_e$  can be observed. This is particularly true for crops, and  
465 Fig. 1 in Jackson et al. (1996) shows that  $Y(d_L)$  and  $R_e$  present a much higher variability for  
466 crops than for temperate grasslands. This difficulty may explain the shortcomings of DIF1  
467 simulations for the 61-Orne département described in Sect. 3.2.1 (Table 4). In particular, the  
468 root density in the top soil layers has a large impact on the water stress modelling. This is  
469 demonstrated by performing an additional DIF1 simulation (DIF1-Uniform) using a uniform  
470 root density profile instead of Eq. (1). Figure 12 shows the evolution of  $B_{ag}$ ,  $SWI_{TOP}(d_R)$  and  
471  $SWI_{TOP}(0.46 \text{ m})$  for the FR-2L, DIF1 and DIF1-Uniform simulations for the 61-Orne  
472 département over the period from April to July 1999. For all the simulations,  $g_m = 1.75 \text{ mm s}^{-1}$   
473 and  $MaxAWC = 225 \text{ mm}$ . The  $B_{ag}$  evolution during the first three months is similar in the  
474 three simulations, with a slightly faster growth for FR-2L. However, while senescence occurs  
475 on mid-July for DIF1, it occurs only at the end of July for FR-2L and DIF1-Uniform. The  
476 early senescence for DIF1 is related to values of  $SWI_{TOP}$  getting close to zero at the top

477 fraction of the root-zone: while  $SWI_{TOP}(0.46\text{ m})$  decreases below the 0.3 critical soil water  
478 stress value (Table 2) at the beginning of July, for DIF1, it never gets below 0.3 in July for  
479 DIF1-Uniform. It must be noted that Fig. 12 shows that root water uptake is reduced earlier  
480 with FR-2L than with DIF1, in relation to a faster plant growth in the FR-2L simulation. For  
481 C3 crops, a drought-avoiding response to soil water stress is simulated, triggering an increase  
482 in WUE (and in the plant growth rate) as soon as  $\theta < \theta_{FC}$ . Since the DIF1 simulations tend to  
483 accumulate water above the field capacity (i.e.  $\theta$  remains longer above  $\theta_{FC}$  than for FR-2L),  
484 the increase in WUE tends to occur later than for FR-2L. Finally, the  $Bag_X$  value for FR-2L  
485 and DIF1-Uniform is higher than for DIF1. This root profile effect also has an impact on the  
486 interannual variability and partly explains the lower  $R^2$  value for DIF1 in Table 4 for this  
487 département.

#### 488 **4.2 Have changes in the representation of photosynthesis an impact on the model** 489 **performance ?**

490 In this section, the impact of the revised vegetation radiative transfer scheme and refreshed  $g_m$   
491 parameter (DIF1-NRT experiment) is discussed. Table 3 shows that while the DIF1-NRT  
492 results are close to those of DIF1 for grasslands, DIF1-NRT tends to outperform DIF1 for C3  
493 crops. Figure 13 presents the simulated  $Bag$  of C3 crops and grasslands for the DIF1 and  
494 DIF1-NRT simulations in the 61-Orne département over the 1994-2010 period. The two  
495 grassland simulations are very similar. On the other hand, the two C3 crop simulations differ  
496 in  $Bag_X$  values. The mean simulated  $Bag_X$  values for C3 crops are  $1.61\text{ kg m}^{-2}$  and  $1.32\text{ kg m}^{-2}$   
497 for DIF1 and DIF1-NRT, respectively. The lower  $Bag_X$  values simulated by DIF1-NRT are  
498 related to the lowest gross primary production simulated by this version of the ISBA-A-gs  
499 model (Carrer et al., 2013). Also, DIF1-NRT simulates shorter growing periods and a slightly  
500 enhanced interannual variability: the ACV (see Sect. 2.7) is equal to 7.4 % for DIF1, and to  
501 8.4 % for DIF1-NRT. For grasslands, the mean simulated  $Bag_X$  values are  $0.46\text{ kg m}^{-2}$  and

502 0.44 kg m<sup>-2</sup> for DIF1 and DIF1-NRT, respectively, and ACV values for DIF1 and DIF1-NRT  
503 are both equal to 30 %.

504 **4.3 Can the ISBA-A-gs model predict the relative gain or loss of agricultural production**  
505 **during extreme years ?**

506 ISBA-A-gs is not a crop model and does not predict yield per se. The background assumption  
507 of this work is that the regional scale above-ground biomass simulated by a generic LSM can  
508 be used as a proxy for GY or DMY in terms of interannual variability. The quantitative  
509 consistency between the simulated biomass and the agricultural statistics was extensively  
510 discussed by Ca12 (Sect. 3.3 and Figs. 12 and 13 in Ca12). For cereals, they considered the  
511 ratio of crop yield to the maximum above-ground biomass, called the harvest index. The later  
512 ranged between 20% and 50% and this was consistent with typical harvest index values given  
513 by Bondeau et al. (2007) for temperate cereals. The same result is obtained in this study (not  
514 shown). For grasslands, Ca12 simulated both managed and unmanaged grasslands. For  
515 managed grasslands, DMY was explicitly simulated and ranged between 0.1 and 0.8 kg m<sup>-2</sup>.  
516 The scatter of the simulated DMY was relatively small, with a standard deviation of  
517 differences with the Agreste DMY of 0.20 kg m<sup>-2</sup>. ISBA-A-gs tended to slightly  
518 underestimate DMY values, with a mean bias of -0.08 kg m<sup>-2</sup>. For unmanaged grasslands, the  
519 simulated *Bag* was 0.17 kg m<sup>-2</sup> higher than the Agreste DMY values, on average. In this  
520 study, unmanaged grasslands were considered, only, and results similar as those of Ca12 were  
521 found (not shown).

522 While the main objective of this work is to evaluate contrasting root water uptake models  
523 using agricultural statistics, it can be investigated how the resulting *Bag<sub>X</sub>* values react to  
524 extreme years (either favourable or unfavourable to agricultural production). The best  
525 simulations result from the optimisation of the MaxAWC parameter. Table 5 summarizes the  
526 true and false detection of favourable and unfavourable years. The latter are defined as  $A_{S, BagX}$

527 or  $A_{S,DMY}$  values higher (lower) than 1.0 (-1.0). The  $A_{S,BagX}$  or  $A_{S,DMY}$  values are based on the  
528 mean time series of Fig. 10. The undetected favourable and unfavourable years are also listed  
529 in Table 5. The best detection performance is obtained by DIF1-NRT for grasslands, with  
530 only 1996 not detected as unfavourable. The worst detection performance is obtained by  
531 DIF1-NRT for C3 crops, with 2003 and 2007 not detected as unfavourable, 1998 and 2004  
532 not detected as favourable, 1997 wrongly detected as unfavourable, and 2008 wrongly  
533 detected as favourable. For grasslands, the extreme years, defined as  $A_{S,DMY}$  values higher  
534 (lower) than 1.5 (-1.5), are 2007 (favourable) and 2003 (unfavourable). These two cases are  
535 correctly identified in the two experiments. For C3 crops, the most favourable years are 2002  
536 and 2009 and the most unfavourable year is 2007. While 2002 and 2009 are correctly  
537 identified in the two experiments, 2007 is not detected. The higher performance in the  
538 representation of extreme years for grasslands than for C3 crops is consistent with the results  
539 of Table 3 showing that significant correlations between  $Bag_X$  and DMY are obtained more  
540 often than between  $Bag_X$  and GY. This can be explained by the more pronounced interannual  
541 variability of the grassland DMY, with ACV = 30 % against ACV values less than 10 % for  
542 the cereal GY. The highest sensitivity of grasslands to climatic conditions is related to their  
543 growing cycle covering a longer period than cereals, and to their MaxAWC values, generally  
544 lower than for cereals (Table 3). Finally, ISBA-A-gs has no direct representation of  
545 agricultural practices and of the cereal GY and the consistency between  $Bag_X$  and GY relies  
546 on the hypothesis that the harvest index (the ratio of GY to  $Bag_X$ ) does not vary much from  
547 one year to another at the considered spatial scale. This issue is discussed in Ca12. For  
548 grasslands, the simulated  $Bag_X$  is more directly representative of DMY. This explains why a  
549 better agreement of the simulations is found with the grassland DMY than with the cereal GY  
550 (Table 3 and Table 5).

#### 551 **4.4 Prospects for better constraining MaxAWC**

552 Ca12 have shown that MaxAWC is the main driver of the interannual variability of *Bag* in the  
553 ISBA-A-gs model. Representing the year-to-year *Bag* variability in a dynamic vegetation  
554 model is a prerequisite to correctly represent surface fluxes at all temporal scales (from hourly  
555 to decadal). Table 3 shows that significant differences in the representation of the *Bag*  
556 interannual variability are triggered by switching from one model option to another. Also, for  
557 a given model option, the median  $g_m$  and MaxAWC values obtained for cereals contrast from  
558 those obtained for grasslands. This is very valuable information for guiding the mapping the  
559 model parameters in future studies. It must be noted that using the interannual variability of  
560 plant growth to assess LSM parameters is a rather new idea. For example, Rosero et al. (2010)  
561 and Gayler et al. (2014) performed an assessment of key parameters of the Noah LSM,  
562 including a version with a dynamic vegetation module, using a set of experimental stations.  
563 However, they did not address the interannual variability of plant growth as their simulations  
564 covered one vegetation cycle, only. Such a short simulation period is not sufficient to  
565 constrain those model parameters which affect the interannual variability of plant growth  
566 (Kuppel et al., 2012).

567 In addition to the intrinsic limitations related to the use of a generic LSM, unable to represent  
568 agricultural practices (see above), uncertainties are generated by the datasets used to force the  
569 LSM simulations. For example, the incoming radiation **in the SAFRAN atmospheric analysis**  
570 can be affected by seasonal biases (Szczypta et al., 2011; Carrer et al., 2012). Since  
571 phenology in ISBA-A-gs is driven by photosynthesis, biases in the incoming radiation can  
572 impact the date of the leaf onset. The impact of errors in the forcing data is probably more  
573 acute for cereals than for grasslands in relation to a shorter growing period. More research is  
574 needed to assess the impact of using enhanced atmospheric reanalyses (Weedon et al., 2011;  
575 Oubeidillah et al., 2014) and proxies for annual agricultural statistics such as gridded

576 maximum LAI values at a spatial resolution of 1 km × 1 km derived from satellite products  
577 (Baret et al., 2013).

578 Another difficulty is that the coarse spatial resolution of agricultural statistics prevents the use  
579 of local soil properties (Sect. 2.3). Models need to be tested at a local scale using data from  
580 instrumented sites. For example, the DIF version of ISBA was tested at a local scale by  
581 Decharme et al. (2011), over a grassland site in southwestern France. However, the soil and  
582 vegetation characteristics at a given site may differ sharply from those at neighboring sites. It  
583 is important to explore new ways of assessing and benchmarking model simulations at a  
584 regional scale. Remote sensing products can be used to monitor terrestrial variables over large  
585 areas and to benchmark land surface models (Szczypta et al., 2014). At the same time, using  
586 in situ observations as much as possible is key, as remote sensing products are affected by  
587 uncertainties. So far, the French annual agricultural yield data are publicly available at the  
588 département scale, only. In order to take advantage of the existing information on soil  
589 properties, an option could be to use satellite-derived LAI products at a spatial resolution of 1  
590 km × 1 km in conjunction with soil maps at the same spatial resolution (e.g. derived from the  
591 Harmonized World Soil Database, Nachtergaele et al. (2012)). Since these products are now  
592 available at a global scale, the methodology explored in this study over metropolitan France  
593 could be extended to other regions.

594 The ISBA-A-gs model is intended to bridge the gap between the terrestrial carbon cycle and  
595 the hydrological simulations (e.g. river discharge). In previous works, the ISBA-A-gs model  
596 was coupled with hydrological models able to simulate river discharge (e.g. Queguiner et al.  
597 2011, Szczypta et al. 2012). While simulating vegetation requires a good description of the  
598 soil water stress, hydrological simulations are sensitive to changes in the representation of the  
599 surface water and energy fluxes. The latter are controlled to a large extent by vegetation. As  
600 suggested by Feddes et al. (2001) and Decharme et al. (2013), the obtained "effective root

601 distribution function" could be validated using river discharge observations by coupling the  
602 LSM with a hydrological model. We will investigate this possibility in a future work. Note  
603 however that the river discharge is often impacted by anthropogenic effects such as dams and  
604 irrigation. Such effects are not completely represented in large scale hydrological models  
605 (Hanasaki et al. 2006).

## 606 5. Conclusions

607

608 The observed cereal GY and permanent grassland DMY production in France from 1994 to  
609 2010 was used in this study to evaluate four contrasting representations of the root water  
610 uptake in the ISBA-A-gs land surface model within SURFEX. A simple representation of the  
611 root-zone soil moisture based on a single bulk reservoir (FR-2L) was compared with  
612 multilayer diffusion models describing the soil water uptake profile. The latter used the  
613 Jackson root vertical distribution equation, with and without additional subroot zone base  
614 flow soil layers. In order to limit the uncertainty related to the lack of knowledge of local  
615 rooting depth conditions, the MaxAWC quantity was retrieved by matching the simulated  
616  $Bag_x$  with the Agreste agricultural statistics, for given vegetation and photosynthesis  
617 parameters. The impact on the results of the representation of the vegetation was assessed  
618 using another representation of the light absorption by the canopy and using refreshed values  
619 of the  $g_m$  photosynthesis parameter. The  $Bag_x$  time series based on the multilayer model  
620 without additional subroot zone base flow soil layers presented correlations with the  
621 agricultural statistics similar to those obtained with FR-2L. On the other hand, adding subroot  
622 zone base flow soil layers tended to degrade the correlations. Overall, a better agreement of  
623 the simulations was found with the grassland DMY than with the cereal GY in relation to  
624 several factors such as (1) the more pronounced interannual variability of the grassland DMY,  
625 (2) the more direct correspondence between  $Bag_x$  and DMY, (3) less variability in the  
626 parameters of the Jackson model than for crops. More research is needed to map the  
627 MaxAWC parameter. In particular, long time series of satellite-derived vegetation products  
628 (e.g. GEOV1, Baret et al. (2013)) could be used in conjunction with soil parameter maps to  
629 constrain MaxAWC. Next steps are to verify that (1) the new model parameters have a  
630 positive impact on the water and carbon fluxes derived from in situ flux-tower observations

631 and satellite products, at a regional scale and at various timescales (hourly to decadal), (2) use  
632 an hydrology model coupled to SURFEX (Szczypta et al., 2012) to assess the impact of the  
633 new MawAWC maps on river discharge.

634

635        **Acknowledgments**

636

637        The doctoral scholarship of N. Canal was funded by Agence Nationale de la Recherche  
638        Technique through a partnership between Météo-France and Arvalis-Institut du Végétal. S.  
639        Lafont was supported by the GEOLAND2 project, co-funded by the European commission  
640        within the Copernicus initiative of FP7 under grant agreement No. 218795, and this study  
641        contributed to the IMAGINES FP7 project No. 311766. The authors would like to thank  
642        Stéphanie Faroux for her help with the SURFEX simulations, as well as the three anonymous  
643        reviewers for their useful comments.

644

645

## References

646

647

648 Agreste: <http://agreste.agriculture.gouv.fr/page-d-accueil/article/donnees-en-ligne>, last access:

649 March 2014, 2014.

650

651 Agreste Bilans: Agreste Chiffres et Données Agriculture No 209, Bilans

652 d’approvisionnements agroalimentaires 2007-2008, 5 pp.,

653 <http://agreste.agriculture.gouv.fr/IMG/file/aliments209.pdf>, last access March 2014, 2007.

654

655 Agreste Conjoncture: Bilan conjoncturel 2007, No 10-11, 40 pp.,

656 <http://agreste.agriculture.gouv.fr/IMG/pdf/bilan2007note.pdf>, last access March 2014, 2007.

657

658 Agreste Infos Rapides: Grandes cultures et fourrages, No 7, Prairies,

659 <http://agreste.agriculture.gouv.fr/IMG/pdf/prairie0711note.pdf>, last access March 2014, 2007.

660

661 Baret, F., Weiss, M., Lacaze, R., Camacho, F., Makhmara, H., Pacholczyk, P., and Smets, B.:

662 GEOV1: LAI and FAPAR essential climate variables and FCOVER global time series

663 capitalizing over existing products, Part 1: Principles of development and production, Remote

664 Sens. Environ., 137, 299–309, 2013.

665

666 Bondeau, A., Smith, P. C., Zaehle, S., Schaphoff, S., Lucht, W., Cramer, W., Gerten, D.,

667 Lotze-Campen, H., Müller, C., Reichstein, M., and Smith, B.: Modelling the role of

668 agriculture for the 20th century global terrestrial carbon balance, *Global Change Biol.*, 13(3),

669 679–706, 2007.

670

671 Boone, A., Masson, V., Meyers, T., and Noilhan, J.: The influence of the inclusion of soil  
672 freezing on simulations by a Soil–Vegetation–Atmosphere Transfer Scheme, *J. Appl.*  
673 *Meteorol.*, 39, 1544–1569, 2000.

674

675 Brisson, N., Gate, P., Gouache, D., Charmet, G., Oury, F.-X. and Huard, F.: Why are wheat  
676 yields stagnating in Europe? A comprehensive data analysis for France, *Field Crops Res.*,  
677 119(1), 201–212, doi:10.1016/j.fcr.2010.07.012, 2010.

678

679 Brut, A., Rüdiger, C., Lafont, S., Roujean, J.-L., Calvet, J.-C., Jarlan, L., Gibelin, A.-L.,  
680 Albergel, C., Le Moigne, P., Soussana, J.-F., Klumpp, K., Guyon, D., Wigneron, J.-P. and  
681 Ceschia, E.: Modelling LAI at a regional scale with ISBA-A-gs: comparison with satellite-  
682 derived LAI over southwestern France, *Biogeosciences*, 6, 1389–1404, 2009.

683

684 Calvet, J.-C.: Investigating soil and atmospheric plant water stress using physiological and  
685 micrometeorological data, *Agr. Forest Meteorol.*, 103, 229–247, 2000.

686

687 Calvet, J.-C., Gibelin, A.-L., Roujean, J.-L., Martin, E., Le Moigne, P., Douville, H. and  
688 Noilhan, J.: Past and future scenarios of the effect of carbon dioxide on plant growth and  
689 transpiration for three vegetation types of southwestern France, *Atmos. Chem. Phys.*, 8, 397–  
690 406, doi:10.5194/acp-8-397-2008, 2008.

691

692 Calvet, J.-C., Lafont, S., Cloppet, E., Souverain, F., Badeau, V. and Le Bas, C.: Use of  
693 agricultural statistics to verify the interannual variability in land surface models: a case study  
694 over France with ISBA-A-gs, *Geosci. Model Dev.*, 5, 37–54, doi:10.5194/gmd-5-37-2012,  
695 2012.

696

697 Calvet, J.-C., Rivalland, V., Picon-Cochard, C., and Guehl, J.-M.: Modelling forest  
698 transpiration and CO<sub>2</sub> fluxes - response to soil moisture stress, *Agr. Forest Meteorol.*, 124,  
699 143–156, doi:10.1016/j.agrformet.2004.01.007, 2004.

700

701 Calvet, J.-C., and Soussana, J.-F.: Modelling CO<sub>2</sub>-enrichment effects using an interactive  
702 vegetation SVAT scheme, *Agr. Forest Meteorol.*, 108, 129–152, 2001.

703

704 Calvet, J.-C., Noilhan, J., Roujean, J., Bessemoulin, P., Cabelguenne, M., Olioso, A. and  
705 Wigneron, J.: An interactive vegetation SVAT model tested against data from six contrasting  
706 sites, *Agr. Forest Meteorol.*, 92, 73–95, 1998.

707

708 Carrer, D., Lafont, S., Roujean, J. L., Calvet, J. C., Meurey, C., Le Moigne, P., and Trigo, I.  
709 F.: Incoming solar and infrared radiation derived from METEOSAT: Impact on the modelled  
710 land water and energy budget over France, *J. Hydrometeorol.*, 13, 504–520, doi:  
711 10.1175/JHM-D-11-059.1, 2012.

712

713 Carrer, D., Roujean, J.-L., Lafont, S., Calvet, J.-C., Boone, A., Decharme, B., Delire, C., and  
714 Gastellu-Etchegorry, J.-P.: A canopy radiative transfer scheme with explicit FAPAR for the  
715 interactive vegetation model ISBA-A-gs: impact on carbon fluxes, *J. Geophys. Res.*  
716 *Biogeosciences*, 118, 1-16, doi:10.1002/jgrg.20070, 2013.

717

718 Deardorff, J. W.: A parameterization of ground-surface moisture content for use in  
719 atmospheric prediction models, *J. Appl. Meteorol.*, 16, 1182–1185, 1977.

720

721 Deardorff, J. W.: Efficient prediction of ground surface temperature and moisture, with  
722 inclusion of a layer of vegetation, *J. Geophys. Res.*, 20, 1889–1903, 1978.

723

724 Decharme, B., Boone, A., Delire, C., and Noilhan, J.: Local evaluation of the Interaction  
725 between Soil Biosphere Atmosphere soil multilayer diffusion scheme using four pedotransfer  
726 functions, *J. Geophys. Res.*, 116, D20126, doi:10.1029/2011JD016002, 2011.

727

728 Decharme, B., Martin, E., and Faroux, S.: Reconciling soil thermal and hydrological lower  
729 boundary conditions in land surface models, *J. Geophys. Res. Atmos.*, 118,  
730 doi:10.1002/jgrd.50631, 2013.

731

732 de Rosnay, P., Calvet, J.-C., Kerr, Y., Wigneron, J.-P., Lemaître, F., Escorihuela, M. J.,  
733 Sabater, J. M., Saleh, K., Barrié, J., Bouhours, G., Coret, L., Cherel, G., Dedieu, G., Durbe,  
734 R., Fritz, N. E. D., Froissard, F., Hoedjes, J., Kruszewski, A., Lavenu, F., Suquia, D., and  
735 Waldteufel, P.: SMOSREX: A long term field campaign experiment for soil moisture and  
736 land surface processes remote sensing, *Remote Sens. Environ.*, 102(3), 377–389,  
737 doi:10.1016/j.rse.2006.02.021, 2006.

738

739 Durand, Y., Brun, E., Merindol, L., Guyomarc'h, G., Lesaffre, B., and Martin, E.: A  
740 meteorological estimation of relevant parameters for snow models, *Ann. Geophys.*, 18, 65–  
741 71, 1993.

742

743 Durand, Y., Giraud, G., Brun, E., Merindol, L., and Martin, E.: A computer-based system  
744 simulating snow-pack structures as a tool for regional avalanche forecasting, *Ann. Glaciol.*,  
745 45, 469–484, 1999.

746

747 Faroux, S., Kaptué Tchuenté, A. T., Roujean, J.-L., Masson, V., Martin, E., and Le Moigne,  
748 P.: ECOCLIMAP-II/Europe: a twofold database of ecosystems and surface parameters at 1  
749 km resolution based on satellite information for use in land surface, meteorological and  
750 climate models, *Geosci. Model Dev.*, 6, 563–582, doi:10.5194/gmd-6-563-2013, 2013.

751

752 Feddes, R. A., Hoff, H., Bruen, M., Dawson, T., de Rosnay, P., Dirmeyer, P., Jackson, R. B.,  
753 Kabat, P., Kleidon, A., Lilly, A., and Pitman, A. J.: Modeling root water uptake in  
754 hydrological and climate models, *Bull. Amer. Meteor. Soc.*, 82(12), 2797-2809, 2001.

755

756 Gate, P., Brisson, N., and Gouache, D.: Les causes du plafonnement du rendement du blé en  
757 France : d’abord une origine climatique, *Evolution des rendements des plantes de grande*  
758 *culture*, Académie d’Agriculture de France, 5 May 2010, Paris, 9 pp., 2010.

759

760 Gayler, S., Wöhling, T., Grzeschik, M., Ingwersen, J., Wizemann, H.-D., Warrach-Sagi, K.,  
761 Högy, P., Attinger, S., Streck, T., and Wulfmeyer, V.: Incorporating dynamic root growth  
762 enhances the performance of Noah-MP at two contrasting winter wheat field sites, *Water*  
763 *Resour. Res.*, 50, 1337-1356, 10.1002/2013wr014634, 2014.

764

765 Gibelin, A.-L., Calvet, J.-C., Roujean, J.-L., Jarlan, L. and Los, S. O.: Ability of the land  
766 surface model ISBA-A-gs to simulate leaf area index at the global scale: Comparison with  
767 satellites products, *J. Geophys. Res.*, 111, D18102, doi:10.1029/2005JD006691, 2006.

768

769 Hanasaki, N., Kanae, S., and Oki, T.: A reservoir operation scheme for global river routing  
770 models, *J. Hydrol.*, 327, 22–41, 2006.

771

772 Jackson, R. B., Canadell, J., Ehleringer, J. R., Mooney, H. A., Sala, O. E., and Schulze, E. D.:  
773 A global analysis of root distributions for terrestrial biomes, *Oecologia*, 108, 389–411,  
774 doi:10.1007/BF00333714, 1996.

775

776 Jacobs, C. M. J.: Direct impact of atmospheric CO<sub>2</sub> enrichment on regional transpiration, PhD  
777 thesis, Agricultural University, Wageningen, 179 pp., 1994.

778

779 Jacobs, C. M. J., van den Hurk, B. J. J. M., and De Bruin, H. A. R: Stomatal behaviour and  
780 photosynthetic rate of unstressed grapevines in semi-arid conditions, *Agr. For. Meteorol.*, 80,  
781 111–134, 1996.

782

783 Jarvis, P. G.: The interpretation of the variations in leaf water potential and stomatal  
784 conductance found in canopy in the field, *Philos. Trans. R. Soc. London B*, 273, 593–610,  
785 doi:10.1098/rstb.1976.0035, 1976.

786

787 Jarvis, N. J.: Simple physics-based models of compensatory plant water uptake: concepts and  
788 eco-hydrological consequences, *Hydrol. Earth Syst. Sci.*, 15, 3431–3446, 2011.

789

790 Krinner, G., Viovy, N., de Noblet-Ducoudré, N., Ogée, J., Polcher, J., Friedlingstein, P.,  
791 Ciais, P., Sitch, S. and Prentice, I. C.: A dynamic global vegetation model for studies of the  
792 coupled atmosphere-biosphere system, *Global Biogeochem. Cycles*, 19, GB1015,  
793 doi:10.1029/2003GB002199, 2005.

794 Kuppel, S., Peylin, P., Chevallier, F., Bacour, C., Maignan, F., and Richardson, A. D.:  
795 Constraining a global ecosystem model with multi-site eddy-covariance data, *Biogeosciences*,  
796 9, 3757–3776, 2012.

797

798 Lafont, S., Zhao, Y., Calvet, J.-C., Peylin, P., Ciais, P., Maignan, F., and Weiss, M.:  
799 Modelling LAI, surface water and carbon fluxes at high-resolution over France: comparison  
800 of ISBA-A-gs and ORCHIDEE, *Biogeosciences*, 9, 439–456, doi:10.5194/bg-9-439-2012,  
801 2012.

802

803 Masson, V., Le Moigne, P., Martin, E., Faroux, S., Alias, A., Alkama, R., Belamari, S.,  
804 Barbu, A., Boone, A., Bouyssel, F., Brousseau, P., Brun, E., Calvet, J.-C., Carrer, D.,  
805 Decharme, B., Delire, C., Donier, S., Essaouini, K., Gibelin, A.-L., Giordani, H., Habets, F.,  
806 Jidane, M., Kerdraon, G., Kourzeneva, E., Lafaysse, M., Lafont, S., Lebeaupin Brossier, C.,  
807 Lemonsu, A., Mahfouf, J.-F., Marguinaud, P., Mokhtari, M., Morin, S., Pigeon, G., Salgado,  
808 R., Seity, Y., Taillefer, F., Tanguy, G., Tulet, P., Vincendon, B., Vionnet, V., and Voltaire,  
809 A.: The SURFEX v7.2 land and ocean surface platform for coupled or offline simulation of  
810 Earth surface variables and fluxes, *Geosci. Model Dev.*, 6, 929–960, doi:10.5194/gmd-6-929-  
811 2013, 2013.

812

813 Nachtergaele, F., van Velthuize, H., Verelst, L., Wiberg, D., Batjes, N., Dijkshoorn, K., van  
814 Engelen, V., Fischer, G., Jones, A., Montanarella, L., Petri, M., Prieler, S., Teixeira, E., and  
815 Shi, X.: Harmonized World Soil Database (version 1.2), 2012, available from:  
816 [http://webarchive.iiasa.ac.at/Research/LUC/External-World-soildatabase/  
817 HWSD\\_Documentation.pdf](http://webarchive.iiasa.ac.at/Research/LUC/External-World-soildatabase/HWSD_Documentation.pdf)

818

819 Noilhan, J., and Mahfouf, J.-F.: The ISBA land surface parameterisation scheme, *Global and*  
820 *Planet. Change*, 13, 145–159, 1996.

821

822 Noilhan, J., and Planton, S.: A simple parameterization of land surface processes for  
823 meteorological models, *Mon. Weather Rev.*, 117, 536–549, 1989.

824

825 Oubeidillah, A. A., Kao, S.-C., Ashfaq, M., Naz, B. S., and Tootle, G.: A large-scale, high-  
826 resolution hydrological model parameter data set for climate change impact assessment for  
827 the conterminous US, *Hydrol. Earth Syst. Sci.*, 18, 67–84, doi:10.5194/hess-18-67-2014,  
828 2014.

829

830 Queguiner, S., Martin, E., Lafont, S., Calvet, J.-C., Faroux, S., and Quintana-Seguí, P.:  
831 Impact of the use of a CO<sub>2</sub> responsive land surface model in simulating the effect of climate  
832 change on the hydrology of French Mediterranean basins, *Nat. Hazards Earth Syst. Sci.*, 11,  
833 2803–2816, doi:10.5194/nhess-11-2803-2011, 2011.

834

835 Quintana-Seguí, P., Le Moigne, P., Durand, Y., Martin, E., Habets, F., Baillon, M., Canellas,  
836 C., Franchisteguy, L., and Morel, S.: Analysis of Near-Surface Atmospheric Variables:  
837 Validation of the SAFRAN Analysis over France, *J. Appl. Meteorol. Clim.*, 47, 92–107,  
838 doi:10.1175/2007JAMC1636.1, 2008.

839

840 Rivalland, V., Calvet, J.-C., Berbigier, P., Brunet, Y., and Granier, A.: Transpiration and CO<sub>2</sub>  
841 fluxes of a pine forest: modelling the undergrowth effect, *Ann. Geophys.*, 23, 291–304, 2005.

842

843 Rosero, E, Yang, Z.-L., Wagener, T., Gulden., L. E., Yatheendradas, S., and Niu, G.-Y.:  
844 Quantifying parameter sensitivity, interaction, and transferability in hydrologically enhanced  
845 versions of the Noah land surface model over transition zones during the warm season. *J.*  
846 *Geophys. Res. Atm.*, 115(D3), D03106, 10.1029/2009jd012035, 2010.

847

848 Sabater, J. M., Jarlan, L., Calvet, J.-C., Bouyssel, F., and De Rosnay, P.: From near-surface to  
849 root-zone soil moisture using different assimilation techniques, *J. Hydrometeorol.*, 8, 194–  
850 206, doi:10.1175/JHM571.1, 2007.

851

852 Schneider, C. L., Attinger, S., Delfs, J. O., and Hildebrandt, A.: Implementing small scale  
853 processes at the soil-plant interface – the role of root architectures for calculating root water  
854 uptake profiles, *Hydrol. Earth Syst. Sci.*, 14, 279–289, 2010.

855

856 Seneviratne, S. I., Corti, T., Davin, E. L., Hirschi, M., Jaeger, E. B., Lehner, I., Orlowsky, B.,  
857 and Teuling, A. J.: Investigating soil moisture-climate interactions in a changing climate: A  
858 review, *Earth-Sci. Rev.*, 99, 3-4, 125-161, doi:10.1016/j.earscirev.2010.02.004, 2010.

859

860 Siqueira, M., Katul, G., and Porporato, A.: Onset of water stress, hysteresis in plant  
861 conductance, and hydraulic lift: Scaling soil water dynamics from millimeters to meters,  
862 *Water Resour. Res.*, 44, W01432, doi:10.1029/2007WR006094, 2008.

863

864 Smith, P. C., De Noblet-Ducoudré, N., Ciais, P., Peylin, P., Viovy, N., Meurdesoif, Y., and  
865 Bondeau, A.: European-wide simulations of croplands using an improved terrestrial biosphere  
866 model: Phenology and productivity, *J. Geophys. Res.*, 115, G01014,  
867 doi:10.1029/2008JG000800, 2010a.

868

869 Smith, P. C., Ciais, P., Peylin, P., De Noblet-Ducoudré, N., Viovy, N., Meurdesoif, Y., and  
870 Bondeau, A.: European-wide simulations of croplands using an improved terrestrial biosphere  
871 model: 2. Interannual yields and anomalous CO<sub>2</sub> fluxes in 2003, *J. Geophys. Res.*, 115,  
872 G04028, doi:10.1029/2009JG001041, 2010b.

873

874 Szczypta, C.: Hydrologie spatiale pour le suivi des sécheresses du bassin méditerranéen, INP  
875 Toulouse, 181 pp., 2012.

876

877 Szczypta, C., Calvet, J.-C., Albergel, C., Balsamo, G., Boussetta, S., Carrer, D., Lafont, S.,  
878 and Meurey, C.: Verification of the new ECMWF ERA-Interim reanalysis over France,  
879 *Hydrol. Earth Syst. Sci.*, 15, 647–666, doi:10.5194/hess-15-647-2011, 2011.

880

881 Szczypta, C., J.-C. Calvet, F. Maignan, W. Dorigo, F. Baret, and P. Ciais: Suitability of  
882 modelled and remotely sensed essential climate variables for monitoring Euro- Mediterranean  
883 droughts, *Geosci. Model Dev.*, 7, 931–946, doi:10.5194/gmd-7-931- 2014, 2014.

884

885 Szczypta, C., Decharme, B., Carrer, D., Calvet, J.-C., Lafont, S., Somot, S., Faroux, S., and  
886 Martin, E.: Impact of precipitation and land biophysical variables on the simulated discharge  
887 of European and Mediterranean rivers, *Hydrol. Earth Syst. Sci.*, 16, 3351-3370,  
888 doi:10.5194/hess-16-3351-2012, 2012.

889

890 Weedon, G. P., Gomes, S., Viterbo, P., Shuttleworth, W. J., Blyth, E., Osterle, H., Adam, J.  
891 C, Bellocq, N., Bouvier, O., and Best, M.: Creation of the WATCH forcing data and its use to

892 assess global and regional reference crop evaporation over land during the twentieth century,  
893 J. Hydrometeorol., 12, 823-848, doi: 10.1175/2011JHM1369.1, 2011.  
894

895

## TABLES

896

897

**Table 1: Nomenclature.**

<b>List of symbols</b>	
ACV	Annual Coefficient of Variation (%)
$A_{S,BagX}(yr)$	Scaled anomaly of $B_{agX}$ of a given year (-)
$A_{S,DMY}(yr)$	Scaled anomaly of DMY of a given year (z score) (-)
$A_{S,GY}(yr)$	Scaled anomaly of GY of a given year (z score) (-)
AWC	Simulated Available soil Water Content ( $kg\ m^{-2}$ )
$B_{ag}$	Simulated above-ground Biomass ( $kg\ m^{-2}$ )
$B_{agX}$	Maximum of simulated above-ground Biomass ( $kg\ m^{-2}$ )
DIF	Multi-layer diffusion model
$d_L$	Depth of a soil layer within the root-zone (m)
DMY	Dry Matter Yields of grasslands ( $kg\ m^{-2}$ )
$D_{max}$	Maximum leaf-to-air saturation deficit ( $kg\ kg^{-1}$ )
$d_R$	Root-zone depth (m)
$F_S$	Soil water stress function (-)
$F_{SC}$	Critical soil water stress (0.3 in this study)
FR-2L	2-layer force-restore model
$F_T$	Plant transpiration flux ( $kg\ m^{-2}\ s^{-1}$ )
$g_m$	Mesophyll conductance in well-watered conditions ( $mm\ s^{-1}$ )
GY	Annual Grain Yields of crops ( $kg\ m^{-2}$ )
LAI	Leaf Area Index ( $m^2\ m^{-2}$ )
LSM	Land Surface Model
MaxAWC	Maximum Available soil Water Content ( $kg\ m^{-2}$ )
NIT	Photosynthesis-driven plant growth version of ISBA-A-gs
$N_L$	Leaf nitrogen concentration (% of leaf dry mass)
NRT	New Radiative Transfer scheme within the vegetation
PAR	Photosynthetically Active Radiation ( $W\ m^{-2}$ )
$R_e$	Root extinction coefficient (-)
SLA	Specific Leaf Area ( $m^2\ kg^{-1}$ )
$S_T$	Root water uptake ( $kg\ m^{-2}\ s^{-1}$ )
WUE	Leaf level Water Use Efficiency (ratio of net assimilation of $CO_2$ to leaf transpiration)
$Y$	Root density profile (-)
<b>Greek symbols</b>	
$\rho$	Water density ( $kg\ m^{-3}$ )
$\theta$	Volumetric soil water content ( $m^3\ m^{-3}$ )
$\theta_{FC}$	Volumetric soil water content at field capacity ( $m^3\ m^{-3}$ )

898

$\theta_{\text{WILT}}$	Volumetric soil water content at wilting point ( $\text{m}^3 \text{m}^{-3}$ )
$\theta_{\text{TOP}}$	Soil moisture content of a top soil layer ( $\text{m}^3 \text{m}^{-3}$ )

898 **Table 2:** Standard values of ISBA-A-gs parameters for C3 crops and grasslands (Gibelin  
 899 et al., 2006).

<i>Plant type</i>	<i>Cuticular conductance</i> ( $g_c$ ) ( $mm\ s^{-1}$ )	<i>Critical soil water stress</i> ( $F_{sc}$ )	<i>Response to drought</i>	<i>Maximum leaf span time</i> ( $\tau_M$ ) ( <i>days</i> )	<i>Minimum leaf area index</i> ( $LAI_{min}$ ) ( $m^2\ m^{-2}$ )	<i>Leaf nitrogen concentration</i> ( $N_L$ ) (% of dry mass)	<i>SLA sensitivity to <math>N_L</math></i> ( $e$ ) ( $m^2\ kg^{-1}\ \%^{-1}$ )	<i>SLA at <math>N_L=0\%</math></i> ( $f$ ) ( $m^2\ kg^{-1}$ )	<i>Fraction of vegetation coverage</i> (%)
C3 crops	0.25	0.3	Avoiding	150	0.3	1.3	3.79	9.84	100
grasslands	0.25	0.3	Tolerant	150	0.3	1.3	5.56	6.73	100

900

901  
 902  
 903  
 904  
 905  
 906

**Table 3:** Median  $g_m$  and MaxAWC values derived for each experiment (<sup>1</sup>) and number of départements where the simulated  $Bag_x$  presents significant correlations (<sup>2</sup>) with the annual yields of Agreste statistics for six cereals (winter wheat, rye, winter barley, spring barley, oat and triticale) and for permanent grasslands in France over the 1994-2010 period.

<i>Plant type</i>	<i>C3 crops</i>					<i>grasslands</i>				
<i>Experiment</i>	FR-2L	DIF1	DIF2	DIF3	DIF1 - NRT	FR-2L	DIF1	DIF2	DIF3	DIF1 - NRT
<i>Median and standard deviation of optimal <math>g_m</math> (<math>mm\ s^{-1}</math>)</i>	<b>1.75</b> 0.40	<b>1.75</b> 0.53	<b>1.75</b> 0.51	<b>1.75</b> 0.53	<b>1.75</b> 0.56	<b>1.38</b> 0.48	<b>1.38</b> 0.49	<b>1.50</b> 0.47	<b>1.25</b> 0.49	<b>1.25</b> 0.42
<i>Median and standard deviation of optimal MaxAWC (mm)</i>	<b>125</b> 54.0	<b>112.5</b> 61.3	<b>81.3</b> 84.0	<b>93.8</b> 63.0	<b>100</b> 64	<b>81.3</b> 55.0	<b>68.8</b> 54.0	<b>75.0</b> 55.0	<b>75.0</b> 58.0	<b>75.0</b> 58.0
<i>Number of départements</i>	45					48				
<i>Number of départements presenting significant correlations (at 1 % and 0.1 % level)</i>	12-5	10-3	6-2	10-3	13-4	34-22	36-20	27-10	33-16	37-19

907 (<sup>1</sup>) the optimisation of  $g_m$  is performed for FR-2L and DIF1-NRT only ; DIF1, DIF2, and  
 908 DIF3 use the same départements-level  $g_m$  values as FR-2L.

909 (<sup>2</sup>) significant correlations at 1 % and 0.1 % level correspond to coefficient of  
 910 determination ( $R^2$ ) values higher than 0.366 and 0.525, respectively.

911

912 **Table 4:** Optimal MaxAWC and squared correlation coefficient ( $R^2$ ) between  $Bag_x$  and  
 913 Agreste for FR-2L and DIF1 simulations at départements where the same cereal Agreste data  
 914 are used and where the correlation between  $Bag_x$  values and the yields of Agreste statistics  
 915 are significant at least at 1% level. The highest MaxAWC and  $R^2$  values at a given  
 916 département are in bold.

<i>Experiment</i>		FR-2L		DIF1	
<i>Département</i>	<i>Cereal</i>	$R^2$	<i>Optimal MaxAWC</i> (mm)	$R^2$	<i>Optimal MaxAWC</i> (mm)
08	oat	0.60	<b>87.5</b>	<b>0.63</b>	75.0
63	winter barley	0.60	<b>112.5</b>	<b>0.63</b>	112.5
18	rye	<b>0.57</b>	<b>225.0</b>	0.54	225.0
86	oat	<b>0.52</b>	<b>87.5</b>	0.51	87.5
11	winter barley	<b>0.53</b>	<b>125.0</b>	0.49	112.5
16	oat	<b>0.46</b>	<b>100.0</b>	0.41	62.5
91	spring barley	<b>0.42</b>	<b>137.5</b>	0.40	112.5
61	triticale	<b>0.53</b>	200.0	0.40	<b>225.0</b>

917

918

919

920

921

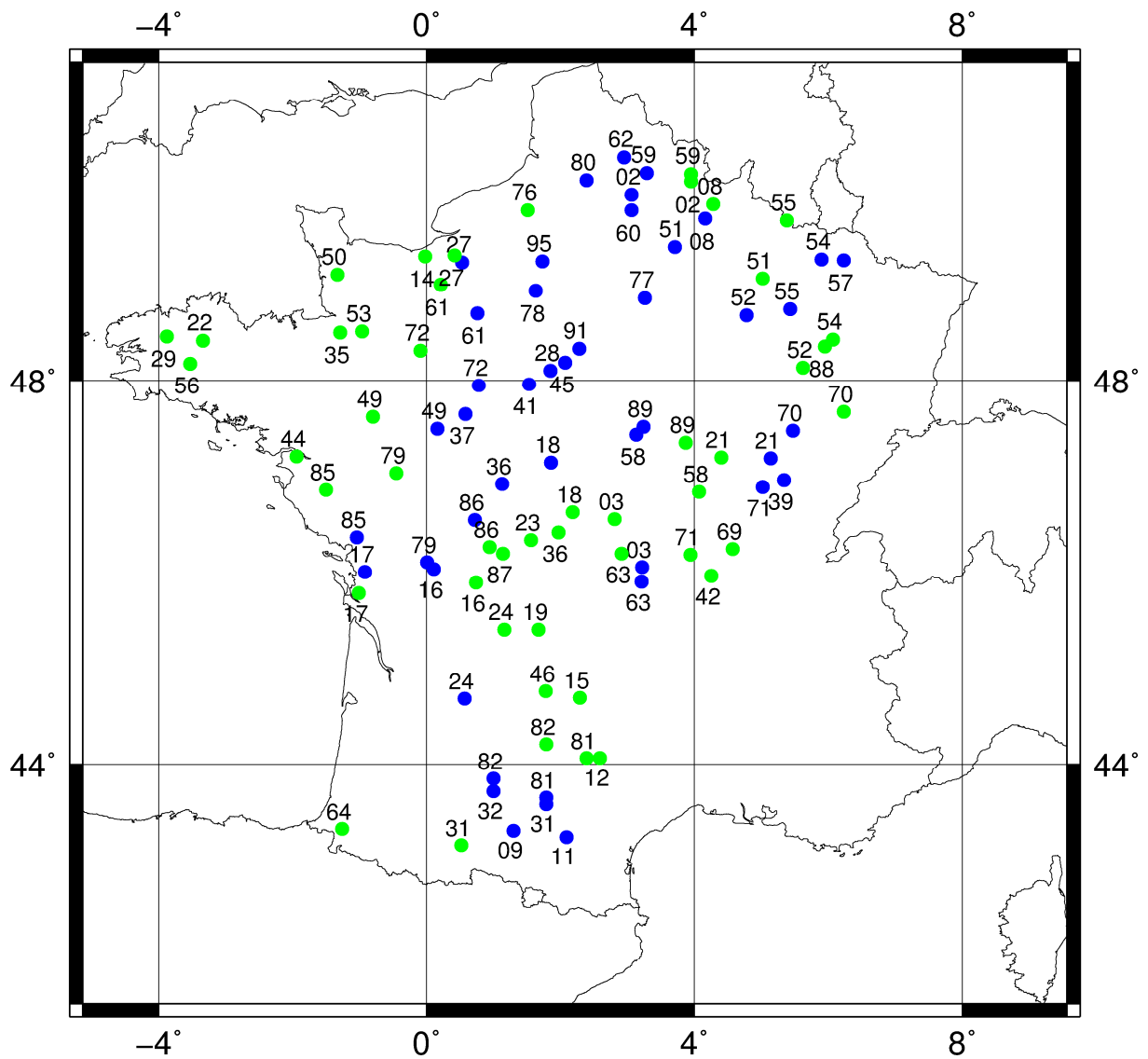
922 **Table 5:** Correspondence between simulated and observed extreme years for  
 923 **départements** with significant correlations ( $R^2$ ) at the 1% level with both FR-2L and DIF1-  
 924 NRT simulations for C3 crops and grasslands as shown in Fig. 10. Favourable (unfavourable)  
 925 years are defined as z-scores  $A_{S,BagX}$  or  $A_{S,DMY}$  higher (lower) than 1.0 (-1.0). Years with  
 926  $A_{S,DMY}$  higher (lower) than 1.5 (-1.5) are in bold.

<i>Plant type</i>	<i>Experiment</i>	<i>Favourable</i>		<i>Unfavourable</i>		<i>Normal (false)</i>	
		<i>True</i>	<i>False</i>	<i>True</i>	<i>False</i>	<i>while favourable</i>	<i>while unfavourable</i>
C3 crops	FR-2L	<b>2002, 2008, 2009</b>			1997, 2010	2004	2001, <b>2007</b>
	DIF1-NRT	<b>2002, 2009</b>	2008	2001	1997	1998, 2004	2003, <b>2007</b>
grasslands	FR-2L	<b>2007, 2008</b>	2000	<b>2003, 2010</b>			1996
	DIF1-NRT	2000, <b>2007, 2008</b>		<b>2003, 2010</b>			1996

927

928

929



931

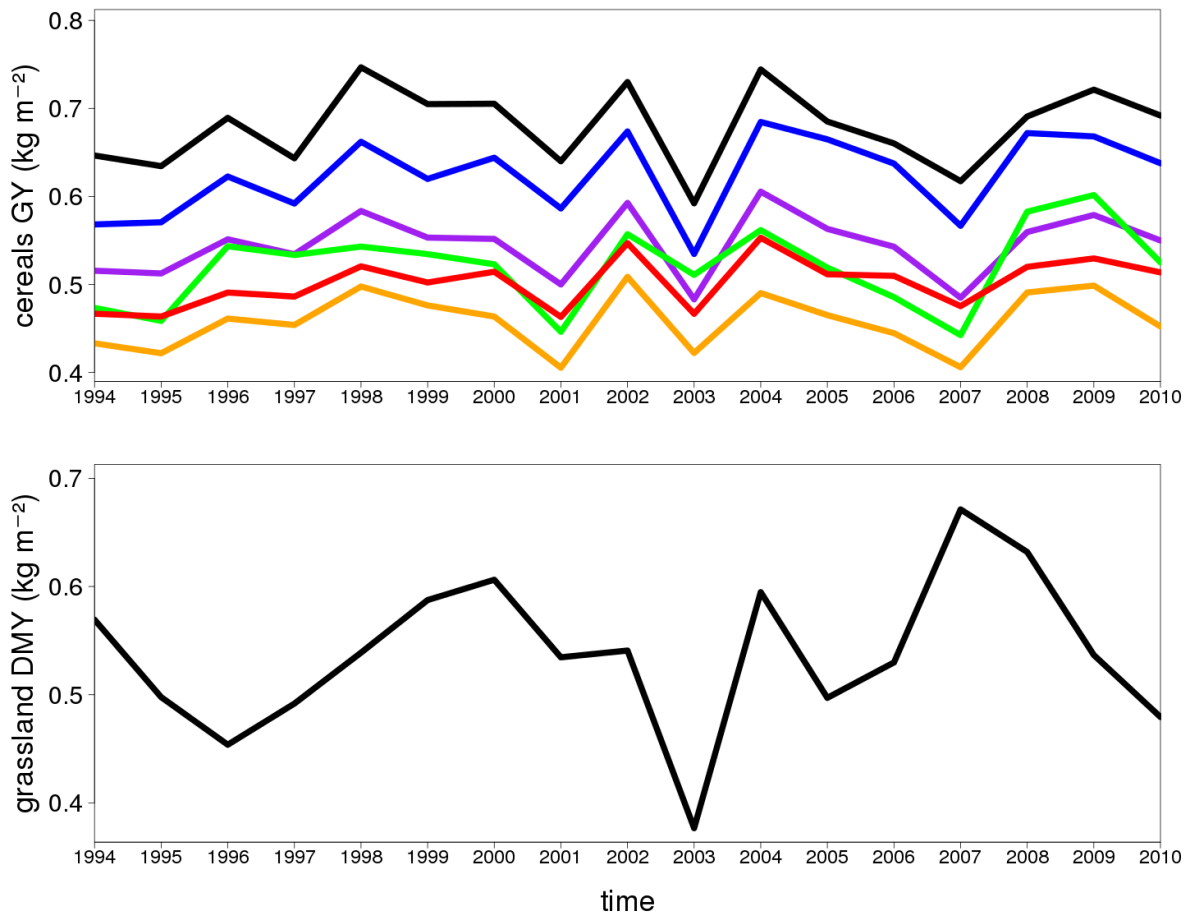
932

933 **Figure 1:** Location of the 45 cropland and 48 grassland 8 km × 8 km grid cells (blue and

934 grassland dots, respectively) and the corresponding département number.

935

936



937

938

**Figure 2:** Averaged annual statistics of Agreste over the 1994-2010 period of (top) grain

939

yields of six cereals (winter wheat in black, rye in red, winter barley in blue, spring barley in

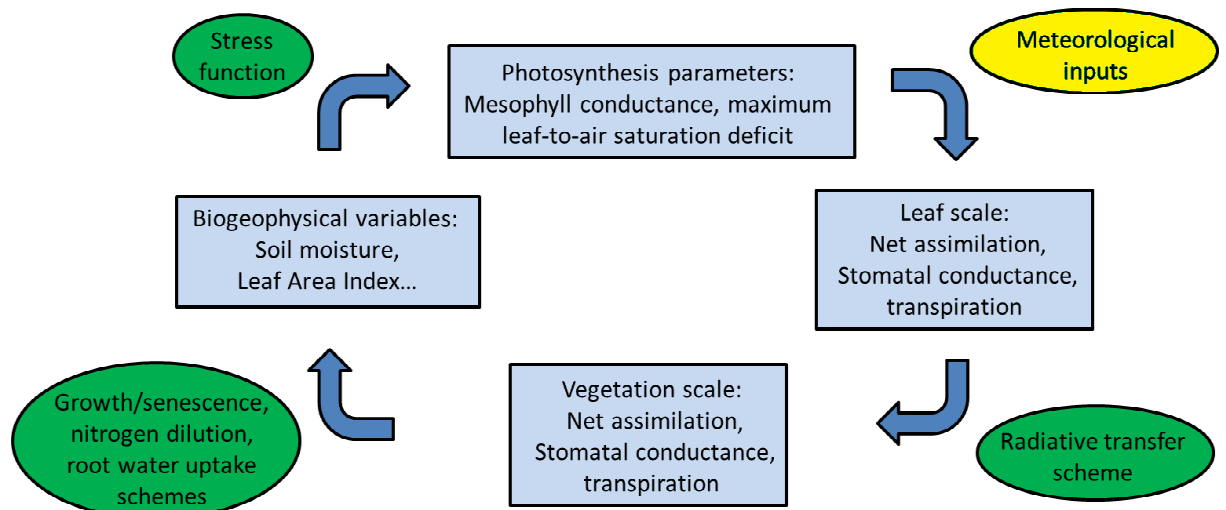
940

green, oat in orange and triticale in purple) over the 45 départements of Fig. 1 and (bottom)

941

dry matter yield of permanent grasslands over the 48 départements of Fig. 1.

942



943

944

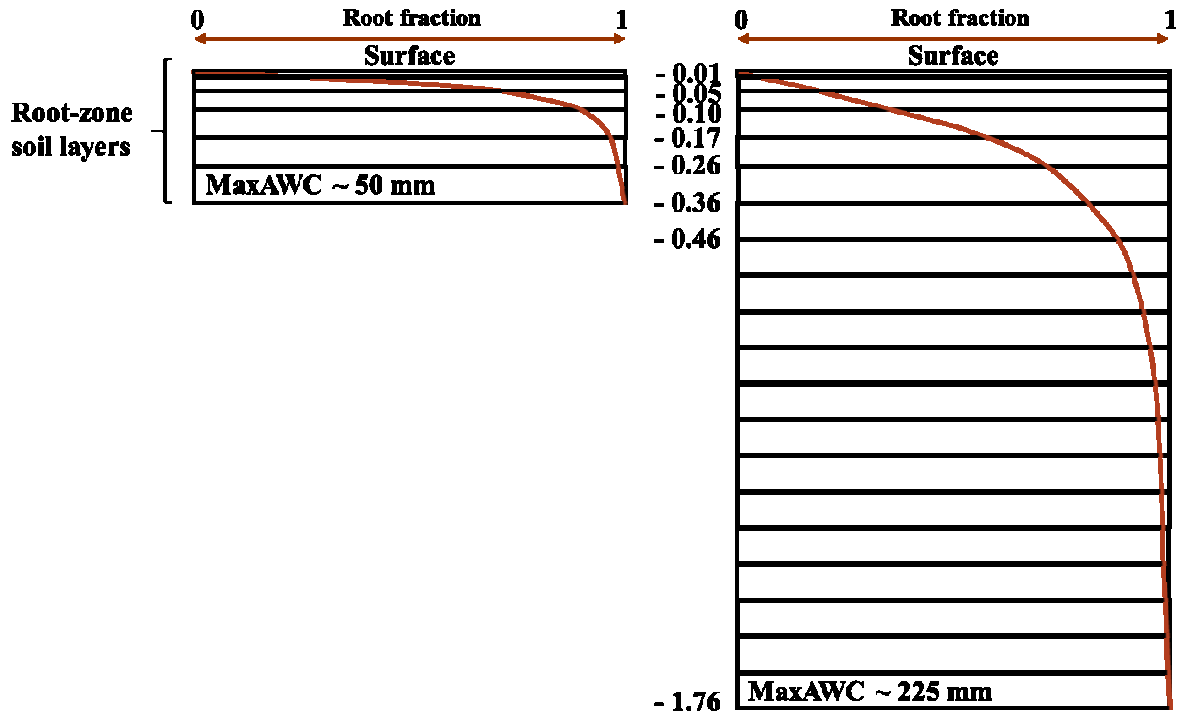
945

**Figure 3:** Relation of biogeophysical variables to leaf-scale and vegetation-scale fluxes in the ISBA-A-gs simulations.

946

947

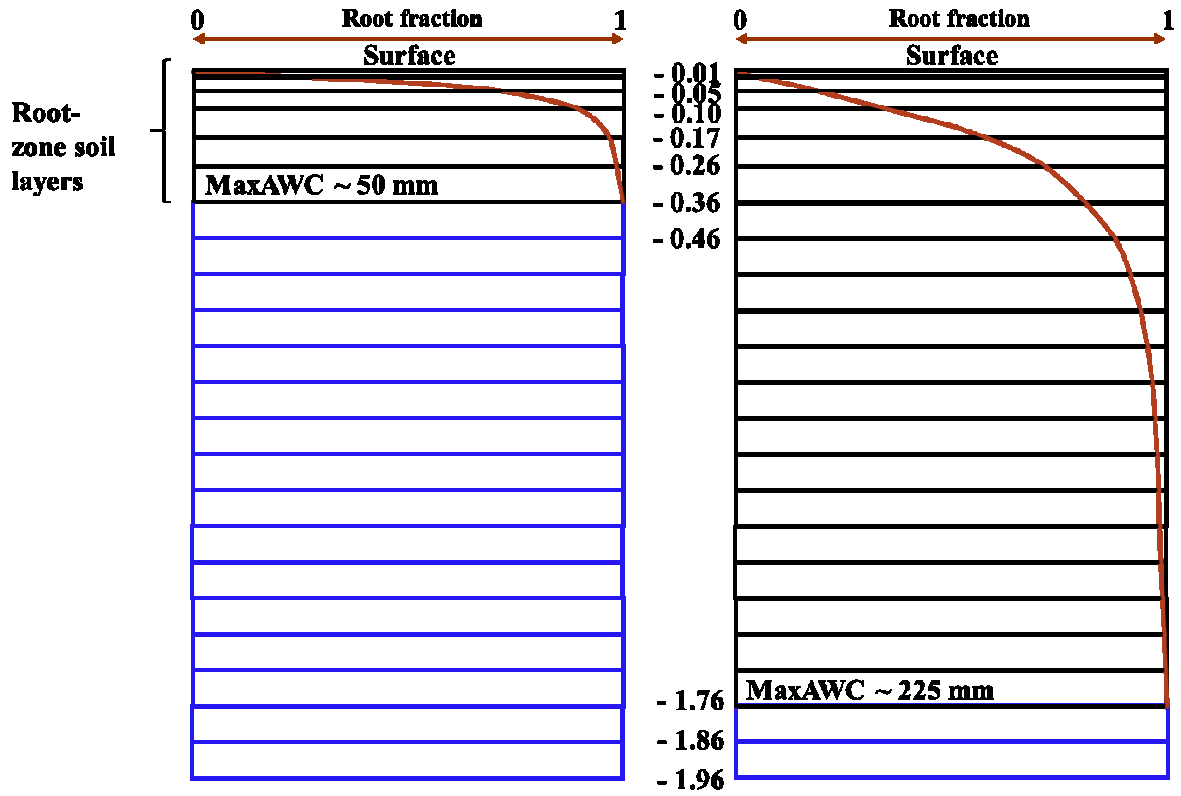
### DIF1



949

950 **Figure 4:** Soil profile of the DIF1 experiment. The soil depth within the root-zone is in  
 951 meters. Only two configurations are represented: for the minimum (left) and maximum (right)  
 952 values of MaxAWC (50 and 225 mm, respectively). The cumulative root density profile for  
 953 crops (Eq. (1) with  $R_e = 0.961$ ) is represented by a brown line. A top soil layer of 1 cm is  
 954 represented.

### DIF2



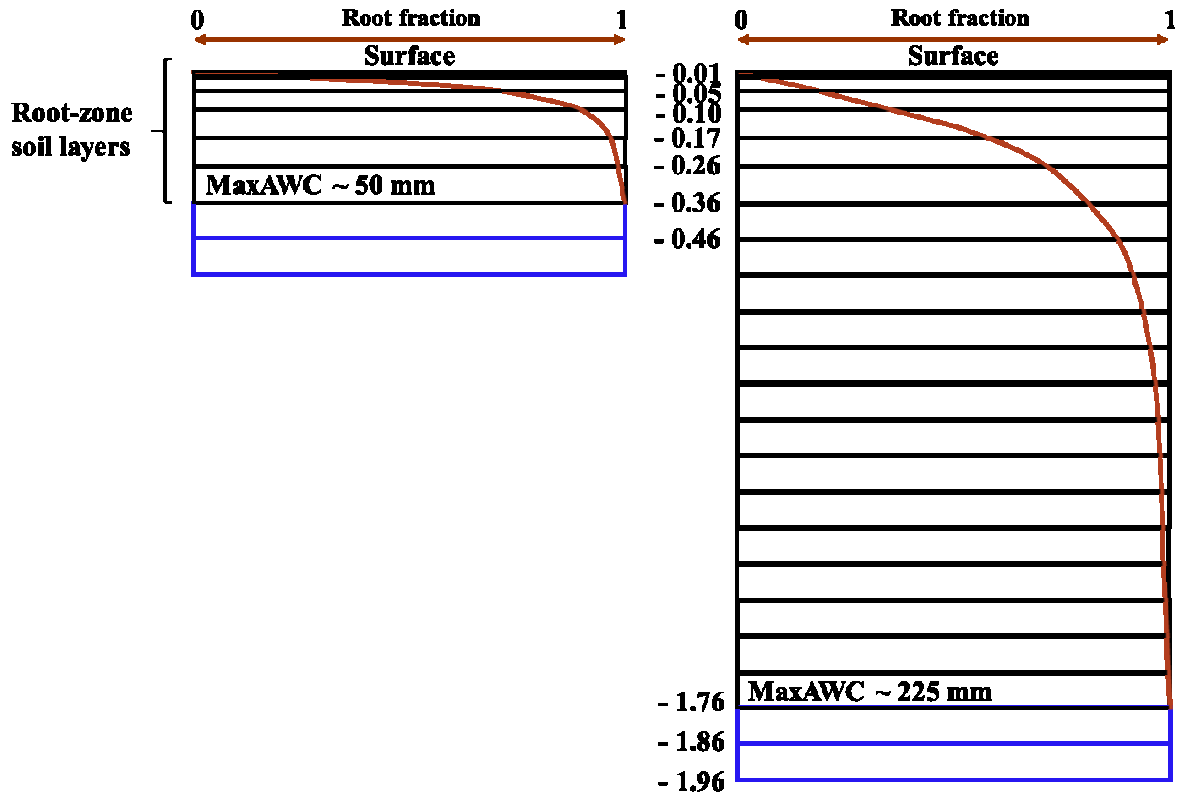
956

957 **Figure 5:** As in Fig. 4, except for DIF2 experiment. Subroot soil layers are added (blue

958 lines), down to a constant soil depth of 1.96 m.

959

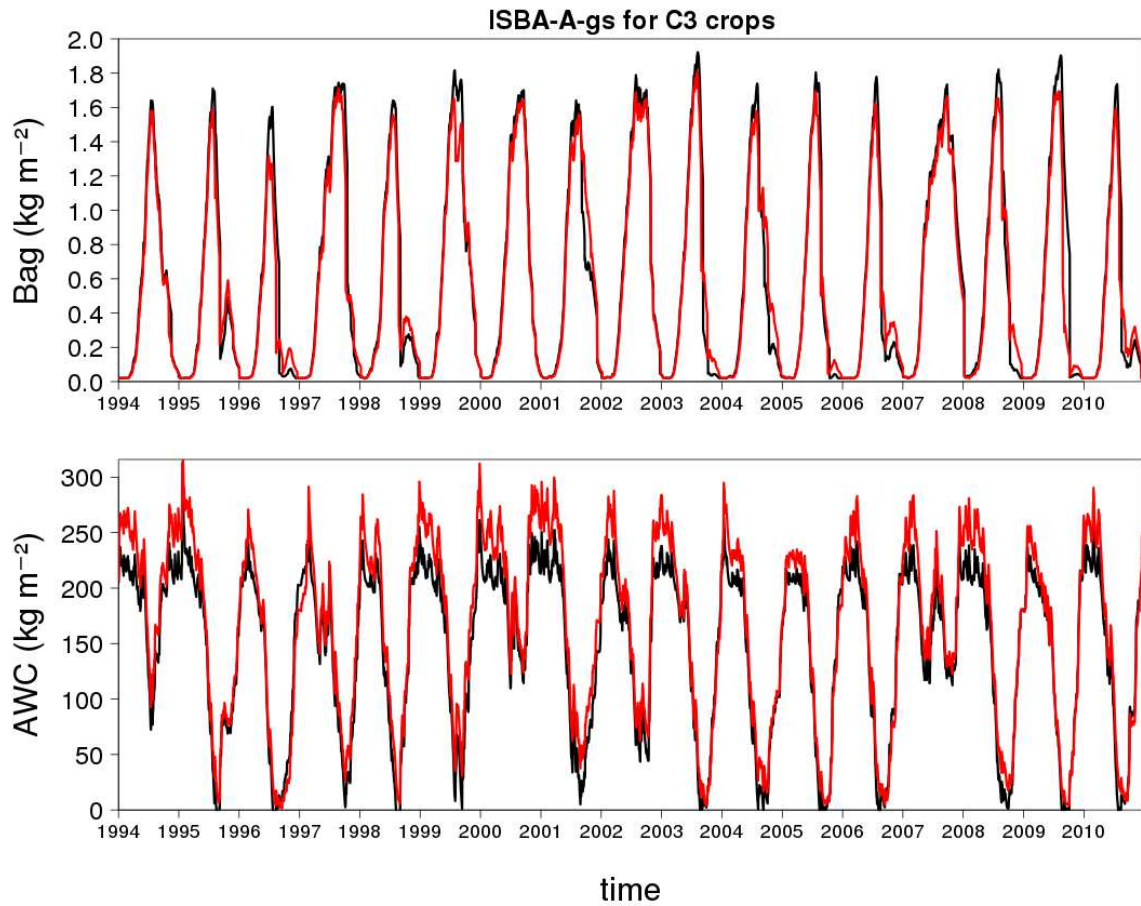
### DIF3



961

962 **Figure 6:** As in Fig. 4, except for DIF3 experiment. Two subroot soil layers of 10 cm are

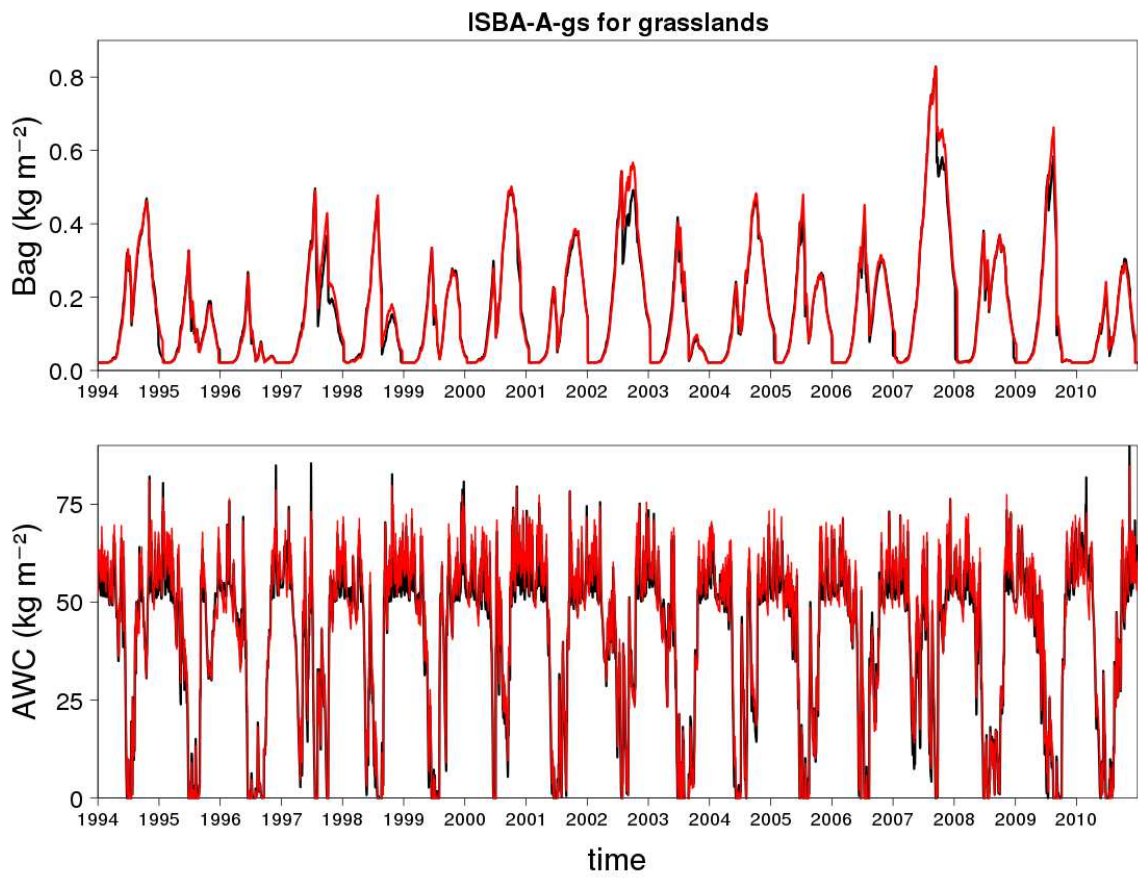
963 added (blue lines).



965

966 **Figure 7:** Simulations over the 1994-2010 period for C3 crops ( $g_m = 1.75 \text{ mm s}^{-1}$ ,  
 967 MaxAWC = 200 mm) in the 61-Orne département of (top) the above-ground biomass and of  
 968 (bottom) the available water content in the root-zone, using the FR-2L and DIF1  
 969 configurations (black and red lines, respectively)

970

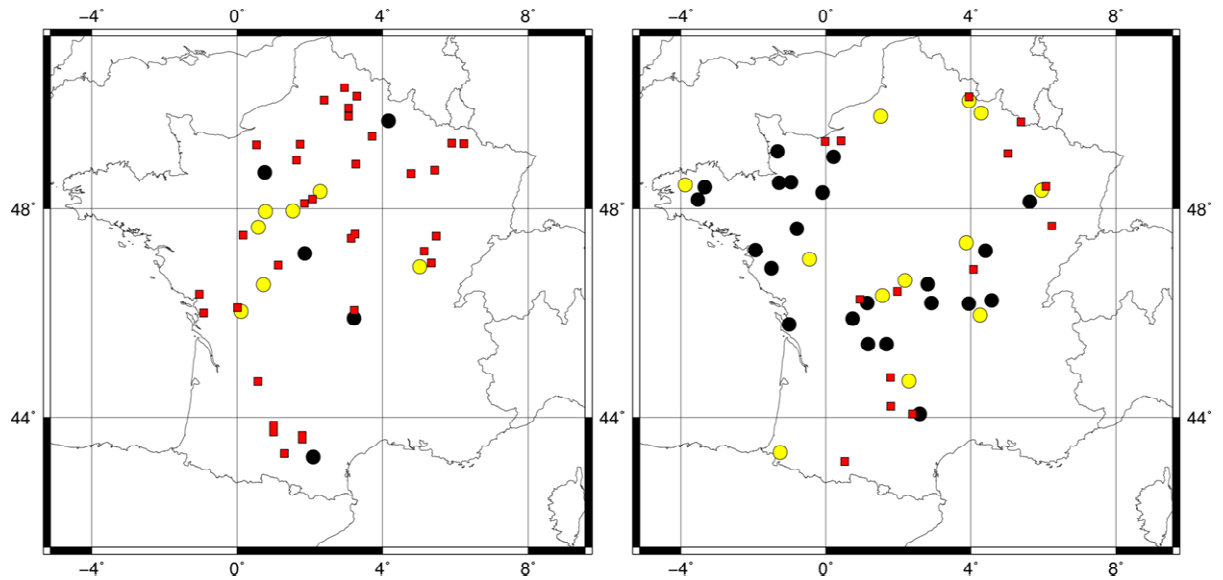


971

972 **Figure 8:** As in Fig. 7, except for grasslands ( $g_m = 0.5 \text{ mm s}^{-1}$ , MaxAWC = 50 mm).

973

974



975

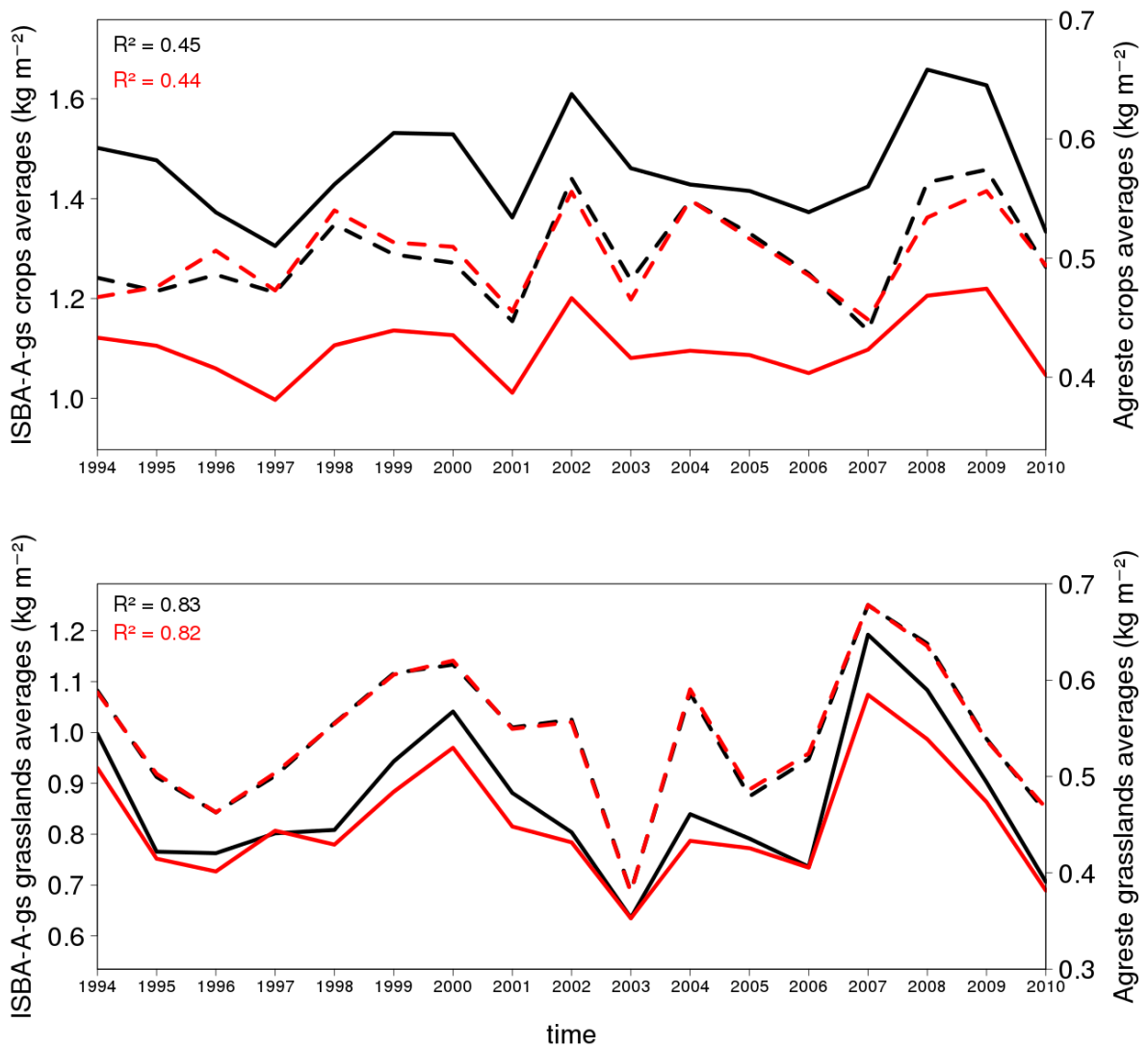
976 **Figure 9:** Best FR-2L simulations vs. Agreste statistics correlation levels obtained for

977 (left) C3 crops and (right) grasslands. Non-significant, significant at the 1% level and

978 significant at the 0.1 % level correlations are indicated in red squares, yellow dots and black

979 dots, respectively.

980

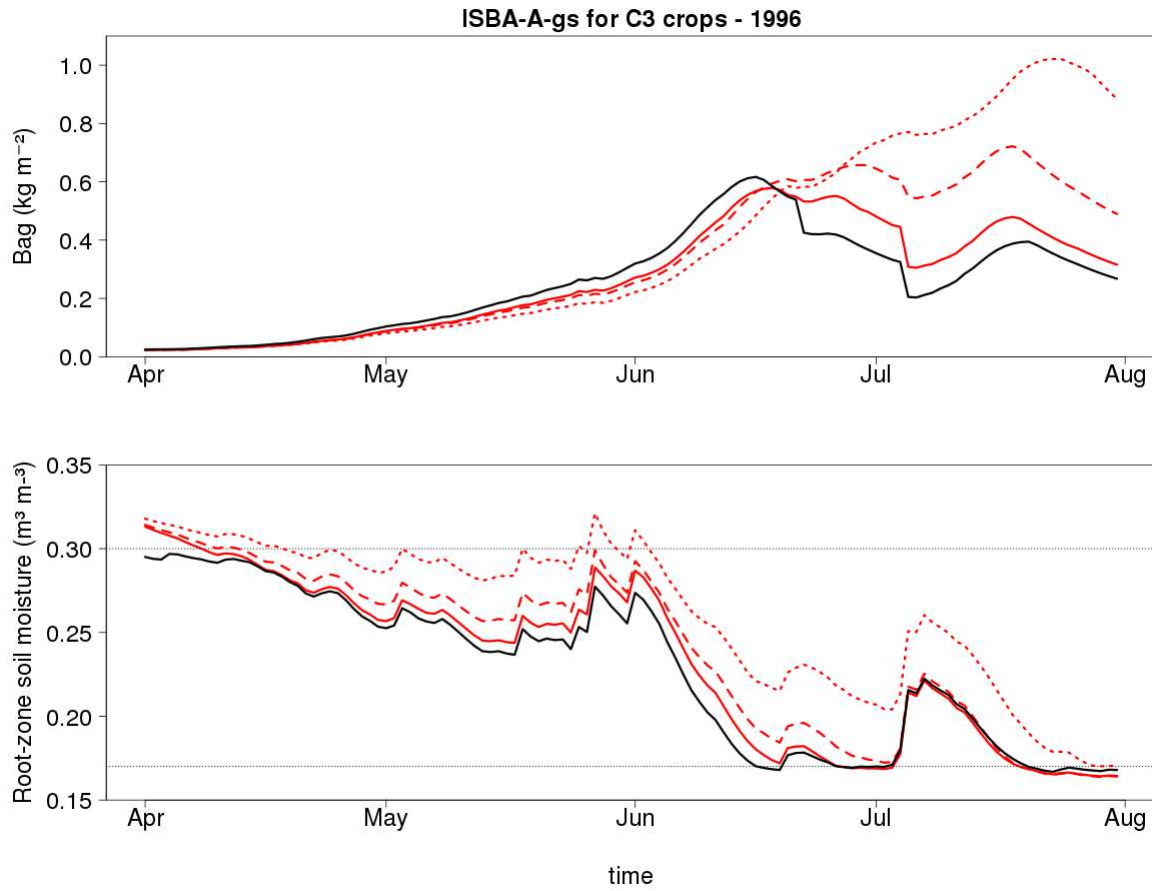


982

983

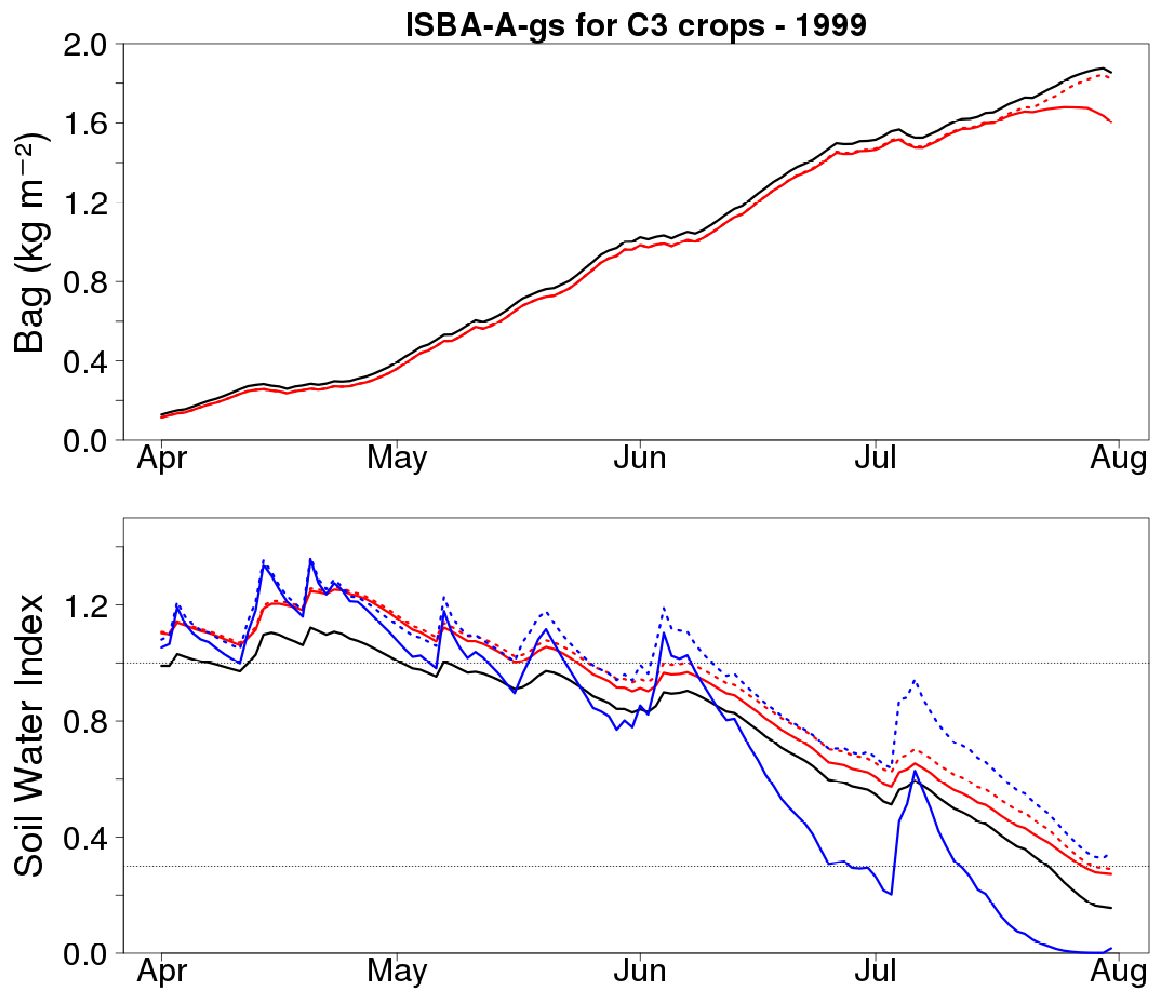
984 **Figure 10:** Averaged simulated yearly  $Bag_X$  values (ISBA-A-gs, solid lines) and  
 985 averaged observed agricultural yields (Agreste, dashed lines) for départements with  
 986 significant correlations ( $R^2$ ) at the 1% level with both FR-2L (black solid line) and DIF1-NRT  
 987 (red solid line) simulations for (top) C3 crop GY and (bottom) grassland DMY.

988



990

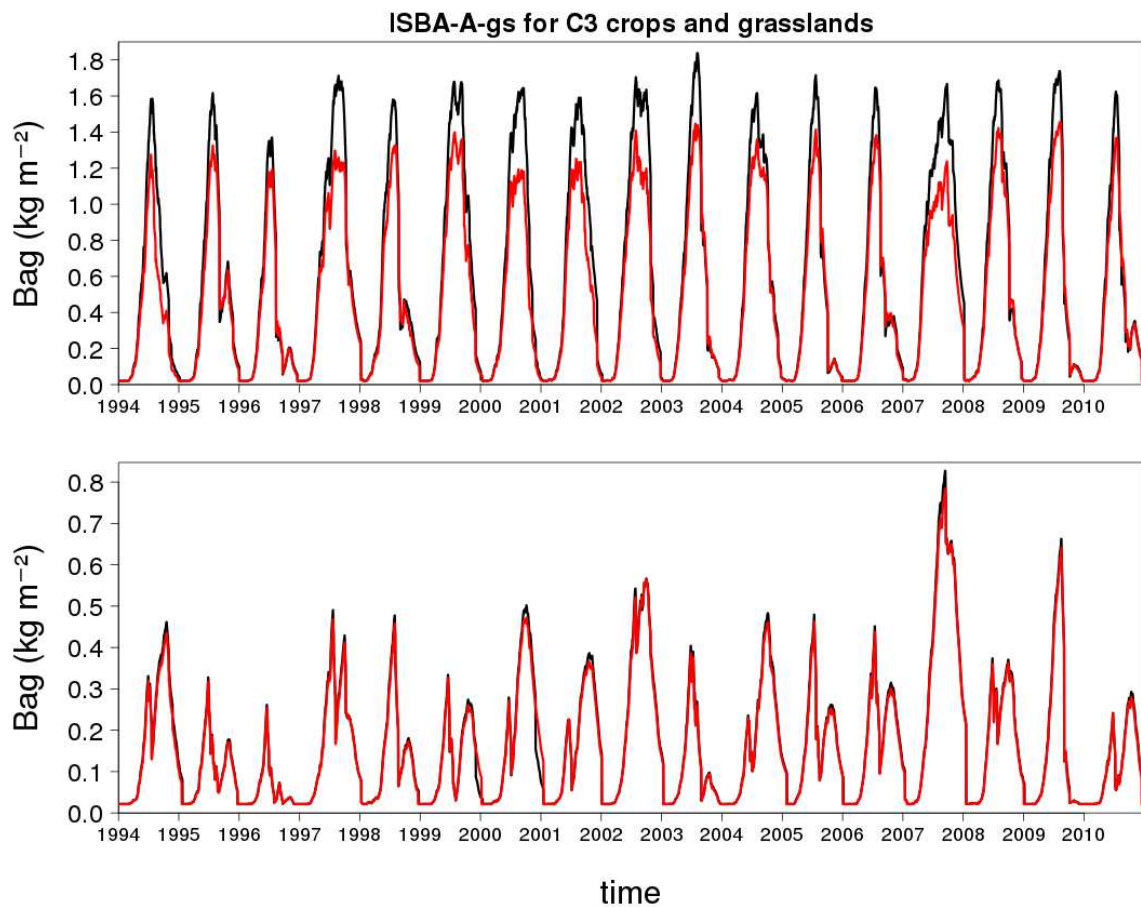
991 **Figure 11:** Simulations in 1996 for C3 crops ( $g_m = 0.5 \text{ mm s}^{-1}$ ,  $\text{MaxAWC} = 75 \text{ mm}$ ) in  
 992 the 08-Ardenne département of (top) above-ground biomass and (bottom) root-zone soil  
 993 moisture in the DIF1, DIF2, DIF3 and FR-2L configurations (red solid, red dotted, red  
 994 dashed, and black lines, respectively). The grey lines indicate the root-zone soil moisture  
 995 values at field capacity and at wilting point.



997

998 **Figure 12:** Simulations in 1999 for C3 crops ( $g_m = 1.75 \text{ mm s}^{-1}$ ,  $\text{MaxAWC} = 225 \text{ mm}$ ,  $d_R$ 999  $= 1.76 \text{ m}$ ) in the 61-Orne department of (top) above-ground biomass, and (bottom)1000  $\text{SWI}_{\text{TOP}}(d_R)$  for FR-2L (black line), DIF1 (red solid line), and DIF1-Uniform (red dotted line),1001 and  $\text{SWI}_{\text{TOP}}(0.46 \text{ m})$  for DIF1 (blue solid line) and DIF1-Uniform (blue dotted line).

1002



1003

1004 **Figure 13:** Simulations over the 1994-2010 period in the 61-Orne département of the  
1005 above-ground biomass for (top) C3 crops ( $g_m = 1.75 \text{ mm s}^{-1}$ , MaxAWC = 225 mm) and  
1006 (bottom) grasslands ( $g_m = 0.50 \text{ mm s}^{-1}$ , MaxAWC = 50 mm) for the DIF1 and DIF1-NRT  
1007 configurations (black and red lines, respectively).

